



Bankoti, K., Rameshbabu, A. P., Datta, S., Goswami, P., Roy, M., Das, D., Ghosh, S. K., Das, A. K., Mitra, A., Pal, S., Maulik, D., Su, B., Ghosh, P., Basu, B., & Dhara, S. (2021). Dual Functionalized Injectable Hybrid Extracellular Matrix Hydrogel for Burn Wounds. *Biomacromolecules*, 22(2), 514–533.  
<https://doi.org/10.1021/acs.biomac.0c01400>

Peer reviewed version

Link to published version (if available):  
[10.1021/acs.biomac.0c01400](https://doi.org/10.1021/acs.biomac.0c01400)

[Link to publication record in Explore Bristol Research](#)  
PDF-document

This is the author accepted manuscript (AAM). The final published version (version of record) is available online via American Chemical Society at <https://doi.org/10.1021/acs.biomac.0c01400>. Please refer to any applicable terms of use of the publisher.

## University of Bristol - Explore Bristol Research

### General rights

This document is made available in accordance with publisher policies. Please cite only the published version using the reference above. Full terms of use are available:  
<http://www.bristol.ac.uk/red/research-policy/pure/user-guides/ebr-terms/>

This document is confidential and is proprietary to the American Chemical Society and its authors. Do not copy or disclose without written permission. If you have received this item in error, notify the sender and delete all copies.

## Dual Functionalized Injectable Hybrid Extracellular Matrix Hydrogel for Burn Wounds

Journal:	<i>Biomacromolecules</i>
Manuscript ID	bm-2020-01400p.R2
Manuscript Type:	Article
Date Submitted by the Author:	20-Nov-2020
Complete List of Authors:	Bankoti, Kamakshi; Indian Institute of Technology Kharagpur, School of Medical Science and Technology Rameshbabu, Arun Prabhu; Indian Institute of Technology Kharagpur, School of Medical Science and Technology Datta, Sayanti ; Indian Institute of Technology Kharagpur, School of Medical Science and Technology Goswami, Piyali ; Indian Institute of Technology Kharagpur Roy, Madhurima ; Indian Institute of Technology Kharagpur Das, Dipankar; Indian Institute of Technology Ghosh, Sudip; Indian Institute of Technology Kharagpur Das, Amit Kumar; Indian Institute of Technology Kharagpur Mitra, Analava; Indian Institute of Technology Kharagpur, School of Medical Science and Technology Pal, Sagar; Indian Institute of Technology (ISM), Dhanbad, Applied Chemistry Maulik, Dhruvajyoti ; Midnapore Medical College and Hospital Su, Bo; University of Bristol, Department of Oral & Dental Science Ghosh, Paulomi; Indian Institute of Chemical Biology, Basu, Bikramjit ; Indian Institute of Science Dhara, Santanu; Indian Institute of Technology Kharagpur, School of Medical Science and Technology

SCHOLARONE™  
Manuscripts

# Dual Functionalized Injectable Hybrid Extracellular Matrix Hydrogel for Burn Wounds

Kamakshi Bankoti<sup>a</sup>, Arun Prabhu Rameshbabu<sup>a</sup>, Sayanti Datta<sup>a</sup>, Piyali Goswami<sup>b</sup>, Madhurima Roy<sup>b</sup>, Dipankar Das<sup>c</sup>, Sudip Kumar Ghosh<sup>b</sup>, Amit Kumar Das<sup>b</sup>, Analava Mitra<sup>d</sup>, Sagar Pal<sup>c</sup>, Dhruvajyoti Maulik<sup>e</sup>, Bo Su<sup>f</sup>, Paulomi Ghosh<sup>g</sup>, Bikramajit Basu<sup>h</sup>, Santanu Dhara<sup>a</sup>

<sup>a</sup>*Biomaterials and Tissue Engineering Laboratory, School of Medical Science and Technology  
Indian Institute of Technology Kharagpur, Kharagpur – 721302, India*

<sup>b</sup>*Department of Biotechnology, Indian Institute of Technology Kharagpur  
Kharagpur – 721302, India*

<sup>c</sup>*Polymer Chemistry Laboratory, Department of Applied Chemistry, Indian Institute of Technology  
(Indian School of Mines), Dhanbad-826004*

<sup>d</sup>*Natural Products Research Laboratory, School of Medical Science and Technology, Indian Institute  
of Technology Kharagpur, Kharagpur 721302, India*

<sup>e</sup>*Department of Surgery, Bankura Sammilani Medical College, Bankura, India*

<sup>f</sup>*Bristol Dental School, University of Bristol, Bristol BS1 2LY, UK*

<sup>g</sup>*Structural Biology and Bioinformatics, CSIR-Indian Institute of Chemical Biology (CSIR-IICB), 4,  
Raja S C Mullick Road, Kolkata –700032, India.*

<sup>h</sup>*Materials Research Center, Indian Institute of Science  
Bangalore, India*

<sup>#</sup>*corresponding author*

*Dr. Santanu Dhara*

*E-mail: [sdhara@smst.iitkgp.ernet.in](mailto:sdhara@smst.iitkgp.ernet.in)*

## Abstract

Low strength and rapid biodegradability of Acellular Dermal Matrix (ADM) restrict wider clinical application as rapid cell delivery platform *in situ*, for management of burn wounds. Herein, extracted ADM was modified by dual cross-linking approach with ionic crosslinking using chitosan (CTS) and covalent cross-linking using an iodine modified 2, 5-dihydro-2,5-dimethoxy-furan (DHF-I) cross-linker; termed as CsADM-Cl. In addition, inherent growth factors and cytokines were found to be preserved in the CsADM-Cl, irrespective of ionic/covalent crosslinking. CsADM-Cl demonstrated improvement in post crosslinking stiffness with decreased biodegradation rate. This hybrid crosslinked hydrogel supported adhesion, proliferation, and migration of human foreskin derived fibroblasts (HFCs) and keratinocytes (HKC). Also, the angiogenic potential of CsADM-Cl was manifested by chick chorioallantoic membrane (CAM) assay. CsADM-Cl showed excellent antibacterial activity against *Escherichia coli* (*E. coli*) and *Staphylococcus aureus* (*S. aureus*). Moreover, CsADM-Cl treated full thickness (FT) burn wounds demonstrated rapid healing marked with superior angiogenesis, well-defined dermal-epidermal junctions (DEJ), mature basket weave collagen deposition, and development of more pronounced secondary appendages. Altogether, the bioactive CsADM-Cl hydrogel established significant clinical potential to support wound healing as an apt injectable antibacterial matrix to encounter unmet challenges concerning critical burn wounds.

**Keywords:** Burn, antioxidant, antibacterial, DHF-I, Chitosan (CTS), Acellular Dermal Matrix (ADM), Collagen (Col)

## 1. Introduction

Burn injuries, a multifaceted acute wound, represent complex inflammatory progression, i.e., intense local inflammation marked by a pronounced propensity to infections. Especially, full thickness (FT) wounds of critical size (diameter > 1 cm), induced by burn, result in rapid loss of liquid and also curtail various vital functions of the skin, leading to development of chronic wounds. Hence, these critical wounds are prone to complications, such as secondary necrosis.<sup>1</sup> Further, healing progression is impeded by restricted blood flow and complex inflammatory reactions, which are stimulated by an initial burn injury.<sup>2</sup> To add up to this slowed down regeneration, these wounds are susceptible to microbial infections and leads to scarring upon healing thus, complicating the treatment modalities.<sup>3</sup>

Hydrogels with *in situ* gelation property are preferred as skin substitute for burn wound management due to their minimal invasiveness and ability to fill the irregular tissue defects. Hydrogels are capable of lending a moist environment that accelerates cell proliferation and collagen deposition in the wound bed along with delivery of bioactive target molecules.<sup>4,5</sup> Bioactive molecules like hormones, cytokines, growth factors, and peptides are reported to promote healing progression. But, their high cost of production limits its application.<sup>6,7</sup> Also, hydrogels with antibacterial activity are widely explored, either by encapsulating antibacterial molecules into the hydrogel, or self-assembling alternate Lys-Val peptides. However, the former causes burst release of antibiotics, whereas in case of latter, the high cost of production, complex preparation protocol, and poor tenability limit its application.<sup>8,9</sup> Iodine is reported to exhibit broad-spectrum antimicrobial properties; hence, is being used frequently in clinics as antiseptic and antimicrobial agent.<sup>10</sup> Notably, the potential of bacterial resistance is significantly reduced due to the alternative mechanism of antimicrobial activity of iodine.<sup>11</sup> For instance, iodine conjugated with polyvinylpyrrolidone known as povidone-iodine has been demonstrated to exhibit antimicrobial property, even against methicillin resistant strains.<sup>12</sup> Altogether, there is an urgent clinical need to develop simple techniques to tackle the stringent pathophysiological requirements of chronic injuries, to induce rapid wound closure and to minimize scar development.

Chitosan (CTS) dressings have been used widely for wound healing purposes, owing to its excellent biocompatibility, biodegradability, antibacterial property, hemostatic nature, and also for drug/biomolecule delivery.<sup>13,14</sup> CTS resembles glycoaminoglycan (GAGs) in structure; however, CTS lacks bioactive signals equivalent to those existing in the extracellular matrix (ECM) for cell attachment, growth, and differentiation. The decoration of cytokines,

1  
2  
3 101 growth factors, signaling molecules, proteins or small cell-binding peptides onto the polymer  
4 surface is used as a strategy to enhance as well as to direct cell responses on biomaterials  
5 102 surfaces.<sup>15-20</sup> In comparison to synthetic matrices that fail to mimic the complexity of ECM *in*  
6 103 *vivo*, biological scaffolds comprised of decellularized ECM (dECM) embodies structures akin  
7 104 to host tissue with superior properties such as a natural 3D morphology, RGDs promoting cell  
8 105 adhesion and proliferation, and inherent biodegradability. dECM has been reported to have  
9 106 potential to guide cell differentiation into appropriate tissue type structures and phenotype.<sup>21-23</sup>  
10 107 Further, dECM supports *in vivo* tissue remodeling and regeneration. Also, ECM degradation  
11 108 products act as chemoattractant for the recruitment of endogenous stem and progenitor cells,  
12 109 and modulates innate immune response.<sup>24,25</sup> dECM scaffolds from various species and tissue  
13 110 have been approved by FDA and are being used clinically for soft tissue repair, wounds  
14 111 management, or heart valve replacement.<sup>26,27</sup> However, decellularized scaffolds may restrict  
15 112 its application due to irregular contours of a wound bed. Thus, *in situ* gelling hydrogels of  
16 113 pepsin-digested dECM will be of great importance. pH-sensitive *in vivo* gelling hydrogels of  
17 114 ECM have been characterized for the preservation of biomolecules in intact form.<sup>28,29</sup> Also,  
18 115 hybrid dECM have been explored for preparing scaffolds, hydrogels, nanofibers, and  
19 116 microspheres.<sup>30-33</sup> However, dECM has weak mechanical strength, have poor biostability and  
20 117 is prone to microbial contamination. Therefore, its use for cell encapsulation and wound  
21 118 healing is questionable. To this end, crosslinking of ECM is being explored in this work. A  
22 119 cross-linking reaction can be performed using chemical reagents (like glutaraldehydes,  
23 120 carbodiimide, genipin), UV light, and enzyme catalysis (such as transglutaminase).<sup>34</sup>  
24 121 Developing bioactive hydrogel with inherent antibacterial activity is a fascinating challenge  
25 122 for the clinical management of burn wounds.  
26 123

27 124 To address this challenge, we have developed injectable soluble acellular dermal matrix  
28 125 (sADM) based hybrid hydrogel platforms based on double crosslinks – forming ionic and  
29 126 covalent bonds for facilitating the recovery of critical FT thermal burn injury in a rat model. A  
30 127 process to dissolve ADM was developed, and hybrid crosslinked hydrogel (CsADM-CI) was  
31 128 formed by blending with CTS, a natural linear biocompatible polysaccharide and iodine  
32 129 modified 2, 5-dihydro-2,5-dimethoxy-furan (DHF-I), a covalent crosslinker. To the best of our  
33 130 knowledge, there is no report of crosslinking ADM using DHF-I, which not only preserves the  
34 131 ECM biological composition and ultrastructure, but also enhances its mechanical strength and  
35 132 control the biodegradation rate as well as provides the unique antibacterial and antioxidant  
36 133 property to the gel. Collagen (Col), being the major protein in the dermal matrix has been  
37 134 explored for its efficacy in wound healing models and therefore, it was selected as control for

1  
2  
3 135 the study. Fabricated hydrogels were characterized for their physio-mechanical attributes and  
4 136 subsequently assessed for cytocompatibility using human foreskin derived fibroblasts (HFCs)  
5 137 and keratinocytes (HKC). Wound healing and angiogenic potential of hydrogels were  
6 138 evaluated *in vitro* using scratch and CAM assay. Wound regeneration was analyzed through  
7 139 histological observations, marker protein expressions and immunostaining of the wound tissue  
8 140 across days of recovery. Furthermore, neo-blood vessel formation, collagen organization and  
9 141 skin appendage formation were determined to evaluate the effect of bioactive cross-linked  
10 142 hybrid hydrogel treatment in the wound repair process.

## 18 143 **2. Experimental section**

### 20 144 *2.1. Decellularization of skin tissue*

22 145 Decellularization of skin was carried out by modifying protocol described  
23 146 elsewhere.<sup>35,36</sup> FT skin was harvested from adult rat (weighing ~150–200 g) and preserved in  
24 147 cold phosphate buffer saline (PBS) containing 0.1% gentamycin, followed by several washing  
25 148 using PBS to remove adhered blood. Samples were processed within 4 h from harvesting.  
26 149 Dermal hair and epidermis were removed using a hypertonic solution (4 g of sodium chloride,  
27 150 605 mg of tris base, and 202.5 mg of EDTA in 100 mL PBS) for 2 to 4 h in an orbital shaker  
28 151 (Thermocon Instruments Private Limited, Bangalore, India), maintained at 37 °C. The isolated  
29 152 dermal layer was denuded using trypsin (0.25%, Thermo Fisher Scientific, USA) and Triton™  
30 153 X-100 (Sigma Aldrich, USA, 0.5 % v/v) treatments; washed several times using PBS. The  
31 154 acellular dermal matrix (ADM) was further treated with a fat digestion solution (chloroform:  
32 155 methanol - 1:1 v/v) for 2 h and subsequently washed with sterile PBS thoroughly and stored at  
33 156 -80 °C. Frozen ADM was lyophilized and pulverized mechanically at 4 °C. Pulverized ADM  
34 157 was solubilized enzymatically (acidic pepsin solution 1 mg/mL) to form soluble ADM (sADM)  
35 158 and stored at -80 °C until required. ADM was characterized by staining with Hematoxylin and  
36 159 Eosin (H&E), anti-Col I antibody (Col I), Alcian Blue (AB), DAPI and DNA quantification,  
37 160 following protocol described in **supporting information**. To investigate the retained proteins  
38 161 after decellularization, the native skin (NS) and ADM were assessed by SDS-PAGE as detailed  
39 162 in **supporting information**. Further, sGAGs and Col were also quantified using colorimetric  
40 163 assays (detailed in **supporting information**). The tissue homogenate prepared aforesaid was  
41 164 analyzed using ELISA Kits (Invitrogen, USA) to investigate the presence of the growth factors  
42 165 (BMP-2, VEGF and TGF-β). Samples were run in triplicate; averaged and standard curve was  
43 166 used to measure concentrations of growth factors in NS and ADM.

1  
2  
3 167 For Col isolation, rat tail was harvested from freshly euthanized adult albino rat  
4  
5 168 (average weight 150-200 g) using protocol described elsewhere.<sup>37</sup> Briefly, the tail was washed  
6  
7 169 with PBS to remove adherent dirt, and the epidermis was removed mechanically using a  
8  
9 170 surgical blade and tweezers. Col fibers from rat tail tendon were cut to smaller fragments and  
10  
11 171 washed successively with acetone and 70 % v/v isopropanol. Rinsed fibers were dissolved in  
12  
13 172 acetic acid (0.02 N) for 48 h at 4 °C and dialyzed against 1 % chloroform water for 1 h and  
14  
15 173 then changed to water for 2 days to remove acetic acid. Col solution was lyophilized after  
16  
17 174 freezing and further stored at -80 °C, until used. Col was characterized using SDS page (details  
18  
19 175 in **supporting information**).

## 20 176 *2.2. Synthesis of iodine modified 2, 5-dihydro-2,5-dimethoxy-furan (DHF-I)*

21  
22 177 DHF-I was synthesized as described elsewhere.<sup>38</sup> Iodine was dissolved in 20% v/v  
23  
24 178 ethanol and mixed with DHF (15 %) at 25 °C. Reaction was allowed to complete in acidic  
25  
26 179 environment for 12 h until reaction color changes from reddish brown to yellow. Subsequently,  
27  
28 180 pH 7 was maintained using sodium hydroxide (NaOH) solution. The product was filtered to  
29  
30 181 remove precipitate, if any. The iodination of DHF was confirmed by proton nuclear magnetic  
31  
32 182 resonance spectroscopy (400 MHz, Advance DAX-400 Bruker, Sweden) using deuterium  
33  
34 183 oxide (Sigma Aldrich, USA) as solvent and the spectrum was compared with the spectrum of  
35  
36 184 pristine DHF.

## 37 185 *2.3. Preparation of hybrid hydrogel*

38  
39 186 CCol-Cl and CsADM-Cl hydrogel were prepared by blending CTS (Molecular weight  
40  
41 187 50,000-190,000 Da; 75-85 % deacetylated, Sigma Aldrich, USA) and Col/sADM using DHF-  
42  
43 188 I as crosslinker. In brief, the blend was neutralized using 0.1 M NaOH in 10X PBS buffer in  
44  
45 189 ice (to maintain temperature 0-10 °C), such that final concentration of polymer and protein in  
46  
47 190 the gel would be 8 mg/mL each and PBS will become 1X. Further, pregel solution was  
48  
49 191 crosslinked using 0.5 % DHF-I, forming a rapid hydrogel. Crosslinked hydrogels were denoted  
50  
51 192 as CCol-Cl and CsADM-Cl, while uncrosslinked hydrogels (without DHF-I) were designated  
52  
53 193 as CCol and CsADM. Tube inversion method was used for measuring gelation time. Also, the  
54  
55 194 pre-gel, not flowing for more than 30s, was taken as a hydrogel. Surface topology of the  
56  
57 195 hydrogels were observed using SEM and fiber networks were analyzed using ImageJ (version  
58  
59 196 6). Further Iodine distribution in crosslinked matrix were confirmed by EDAX mapping of  
60  
197 Iodine on CCol-Cl/CsADM-Cl hydrogel. In brief, the hydrogels were coated on coverslips and  
198 kept at 37 °C for 15 min to facilitate gelation. Coated coverslips were dried in desiccator and



199 stored *therein* until SEM analysis was carried out after gold coating of the sample to avoid  
200 moisture.

#### 201 *2.4. Immunohistochemistry (IHC) of hydrogel*

202 To assess retention of important matrix proteins and biomolecules after crosslinking,  
203 IHC was performed on NS, ADM, CsADM, and CsADM-Cl. The primary antibodies against  
204 Col-I (Abcam), fibronectin, vascular endothelial growth factor (VEGF), transforming growth  
205 factor- $\beta$  (TGF- $\beta$ ), interleukin-8 (IL-8), and monocyte chemoattractant protein-1 (MCP-1) (all  
206 Santa Cruz Biotechnology, Inc.) were used. The stained samples were imaged under an  
207 inverted fluorescent microscope (AxioVision, Zeiss, Germany).

#### 208 *2.5. Rheological characterization*

209 CCol, CsADM, CCol-Cl and CsADM-Cl were further characterized for gelation  
210 kinetics using Dynamic Shear Rheometer (DSR+, Malvern, U.K.). Pregel solution was formed  
211 by blending CTS with Col/sADM. Gelation kinetics was assessed by rheometer using parallel  
212 plate geometry, a gap of 200  $\mu\text{m}$  and parallel plate of 25 mm were maintained in all the  
213 experiments. Pre-gel solution were neutralized in ice and loaded immediately to pre-cooled  
214 rheology plate at 15  $^{\circ}\text{C}$ . Mineral oil was used to reduce evaporation from edges and temperature  
215 was raised to 37  $^{\circ}\text{C}$  to induce gelation. Gelation kinetics was studied by applying constant  
216 frequency (1 Hz) and strain (0.1 %). Further, the hydrogels were subjected to small oscillatory  
217 frequency sweep at strain 0.5 % and frequency 0.5 to 20 Hz.

#### 218 *2.6. FTIR*

219 Fourier transformer infrared (FTIR) spectroscopy of the hydrogels was performed in  
220 ATR mode in the wavelength range of 500–4000  $\text{cm}^{-1}$  on a Thermo Nicolet Spectrophotometer  
221 (Model NEXUS-870; Thermo Nicolet Corporation, Madison, WI). Vacuum dried hydrogels  
222 (CCol, CsADM, CCol-Cl and CsADM-Cl) were stored carefully in desiccators to avoid  
223 moisture, before FTIR spectra were recorded.

#### 224 *2.7. Iodine dynamic release kinetics*

225 To study the iodine dynamic release from cross-linked variant CsADM-Cl, hydrogel  
226 was incubated in PBS and buffered enzymatic solution (Collagenase I, Sigma, USA) to imitate  
227 *in vivo* conditions. Supernatant was collected at predetermined period i.e. 2, 4, 6, 12, 24, 48,  
228 72 and 96 h. In brief, the pre-gel 1mL was gelled for 24 h in 37  $^{\circ}\text{C}$  and the hydrogel was

1  
2  
3 229 incubated with 10 mL of PBS/collagenase I (125 U/ mL) in 0.1 M Tris base, 0.25 M CaCl<sub>2</sub>  
4 230 with pH maintained at 7.4 in 37 °C maintaining incubator and stirring using mechanical stirrer  
5 231 at 100 rpm (Schematic representation in Figure S4). At predetermined period 400 µL  
6 232 supernatant was extracted from sample vial and replenished with 400 µL of fresh PBS/buffered  
7 233 enzymatic solution to maintain constant volume. Samples were centrifuged, collected  
8 234 supernatant was filtered through 0.2 µm syringe filter and stored at -80 °C until analyzed using  
9 235 Dionex ICS 2100 (Thermo Scientific, USA).

## 16 236 2.8. Antioxidant efficiency of hydrogels

19 237 The *ex-vivo* antioxidant efficacy of CCol-Cl and CsADM-Cl was assessed by  
20 238 measuring their potential to scavenge the stable 1, 1-diphenyl-2-picrylhydrazyl (DPPH, Sigma  
21 239 Aldrich, USA) free radical, following the protocol described elsewhere with minor  
22 240 modifications.<sup>39</sup> The uncrosslinked/crosslinked hydrogels were homogenized to powder using  
23 241 liquid nitrogen. Briefly, DPPH (3.0 mL, 100 µM) and dispersion of samples (containing 5 mg)  
24 242 in methanol were stirred and incubated in a dark place for 30 min. Then, DPPH scavenging  
25 243 were assessed by measuring the absorbance a UV–Vis spectrophotometer (Multiskan™ GO  
26 244 Microplate Spectrophotometer, Thermo Fisher Scientific, USA) at 517 nm and calculated using  
27 245 the following equation:

$$34 \quad \text{DPPH scavenging \%} = \frac{A_B - A_H}{A_B} \times 100$$

35 246  
36 247 Where, A<sub>B</sub> is the absorption of the blank (DPPH in methanol) and A<sub>H</sub> the absorption of  
37 248 the hydrogel (hydrogel with DPPH in methanol). Samples were run in triplicate and averaged.

## 41 249 2.9. Haemocompatibility

42 250 The hemocompatible characteristics of the hydrogels was evaluated using the  
43 251 heparinized blood, following protocol described elsewhere.<sup>40</sup> Heparinized blood was  
44 252 centrifuged to obtain RBC pellet and the pellet was subsequently washed thrice with (4-(2-  
45 253 hydroxyethyl)-1-piperazine ethane sulfonic acid (HEPES; 5 mM) buffer containing sodium  
46 254 chloride (150 mM). To hydrogels/normal saline (negative control)/1% Triton™ X-100  
47 255 (positive control), 200 µl of the suspension (5% diluted anticoagulant blood solution in 0.9%  
48 256 NaCl solution) was added and further incubated for 30 min at 37 °C. The supernatant was  
49 257 collected post-centrifugation (1000 g, 10 min) and absorbance was recorded at 540 nm (n=3).  
50 258 The % hemolysis was evaluated using the following equation:

1  
2  
3 259 **Hemolysis (%) = [(absorbance of sample - absorbance of negative control)/ (absorbance**  
4 **of positive control - absorbance of negative control)] x 100**  
5 260

6  
7 261 *2.10. Bacterial inhibition*  
8

9  
10 262 The hydrogels were prepared in sterile 24 well plates and washed with sterile PBS to ensure  
11 263 sterility of the samples before conducting antibacterial efficacy.<sup>41</sup> *Staphylococcus*  
12 264 *aureus* (*S. aureus*) (N315) and *Escherichia coli* (*E. coli*) (DH5 $\alpha$ ) strains were  
13 265 taken for the present study. 20  $\mu$ l bacterial suspensions ( $5 \times 10^7$  CFU mL<sup>-1</sup>) were spread onto  
14 266 each hydrogel (CCol, CsADM, CCol-Cl and CsADM-Cl) in a tissue culture plate and incubated  
15 267 for 2 h at 37 °C, relative humidity >90%. To collect bacterial survivors, post 2 h treatment,  
16 268 sterile PBS (1 mL) was added and a series of 10-fold dilution was prepared, followed by plating  
17 269 out in Luria Bertani agar. Survivor bacteria were allowed to grow for 16 - 18 h by incubating  
18 270 at 35 °C and counted for colony-forming units (CFU). Tissue culture plate (TCP) served as a  
19 271 control and was processed in similar fashion like other samples. The results are expressed as -  
20 272 **Log reduction (%) = log (cell count of control) - log (survivor count on hydrogel) (100)/**  
21 273 **log (cell count of control)**  
22  
23  
24  
25  
26  
27  
28  
29  
30

31 274 For Live/Dead assay, the chosen bacterial strains were seeded on hydrogels as aforesaid  
32 275 and post-incubation, the nutrient broth was removed. Subsequently, the hydrogels were washed  
33 276 with PBS, Live/Dead solution (3  $\mu$ g/mL ethidium bromide and 5  $\mu$ g/mL acridine orange in PBS)  
34 277 was added to each hydrogel and the plates were incubated at 37 °C for 15 min in the dark. After  
35 278 this, the samples were washed with PBS and imaged using Carl Zeiss fluorescence microscope.  
36 279 Experiment was repeated twice in triplicate and data represent average with standard deviation.  
37  
38  
39  
40  
41

42 280 *2.11. Chick chorioallantoic membrane (CAM assay)*  
43  
44

45 281 The angiogenic potential of the hydrogel (CCol-Cl and CsADM-Cl) was investigated  
46 282 by CAM assay, following protocol reported earlier.<sup>33</sup> Fertilized chicken eggs procured  
47 283 (regional poultry farm, Midnapore, West Bengal, India) were cleaned with warm sterile saline,  
48 284 wiped and incubated at 37°C, 60% humidity. After 3 days, sterilized hydrogels (CCol-Cl and  
49 285 CsADM-Cl) were implanted onto the CAM of the eggs with careful sterile dissection making  
50 286 a small window away from the embryo (n=3). The window was resealed through adhesive tape  
51 287 and the eggs were further incubated until day 8 of embryo development. Post- incubation  
52 288 period, the hydrogel treated CAM membrane was photographed and analyzed for angiogenesis.  
53  
54  
55  
56  
57  
58  
59  
60

1  
2  
3 289 The vessels approaching toward the scaffold was counted by three independent observers and  
4 results were reported by taking the average.  
5  
6

## 7 291 *2.12. Cell culture study*

### 8 292 *2.12.1. Conditioning media and related assays*

9  
10  
11 293 The matricryptic peptides or cytokines, major portion of eluted components may affect  
12 scaffold cellularization and remodeling. All materials were processed under sterile condition  
13 294 in a blinded fashion. Each hydrogel was weighed equally and minced using a sterile razor;  
14 295 subsequently, minced hydrogels were placed in six-well plates. Dulbecco's Minimum Essential  
15 296 Medium (DMEM) high glucose (Life Technologies, USA) was added to minced hydrogels  
16 297 (ratio: 50 mg hydrogel/mL medium) and incubated at 37 °C, 5% CO<sub>2</sub>. Untreated medium was  
17 298 processed simultaneously and acted as a control for the study. 72 h post incubation, the media  
18 299 was centrifuged (16,000 g for 10 min) for removing hydrogel particles and untreated medium  
19 300 was added to attain a final concentration of 25 mg crushed hydrogel/mL medium. The  
20 301 morphological changes of HFCs/HKC was documented using Rhodamine and DAPI  
21 302 (Invitrogen™, Thermo Scientific, USA) staining.<sup>42</sup> 15,000 cells/coverlip were seeded and  
22 303 cultivated for predetermined period i.e. 72 h. Post preset period, cells were fixed using 4%  
23 304 PFA, stained for Rhodamine & DAPI and images were recorded using fluorescence microscope  
24 305 (Carl Zeiss) for evaluating cytocompatibility of different hydrogel's conditioned media; where  
25 306 complete media acted as a control for the study.  
26 307

27 308 The conditioning media was also subjected to scratch assay using HFCs/HKCs to study  
28 309 the role of conditioning media in supporting the migration potential of HFCs/HKC. Scratch  
29 310 assay was performed to evaluate *in vitro* wound healing potential of the conditioning media of  
30 311 the hydrogel. In brief, HFCs were grown till the formation of the monolayer; then  
31 312 wound/scratch was created using sterile 200 μm tip. The plates were washed carefully twice  
32 313 with sterile PBS to remove any unattached cells on a plate and wound area. The complete media  
33 314 was replaced with conditioning media and micrographs were obtained after a predetermined  
34 315 period (i.e HFC – 6 h and 12 h; HKC – 12 h and 24 h). Number of migrated cells in denuded  
35 316 area was also calculated for both HFCs and HKCs by three independent observers and the  
36 317 results were demonstrated as mean ± standard deviation (SD).  
37

### 38 318 *2.12.2. Direct Cytotoxicity Testing*

#### 39 319 *2.12.2.1. MTT Assay*

1  
2  
3 320 Cytotoxicity of hydrogels were evaluated using 3-(4,5-dimethyl-2-thiazolyl)-2,5-  
4 321 diphenyl-2H-tetrazolium bromide (MTT) assay by directly cultivating HFCs/HKCs on CCol,  
5 322 CsADM, CCol-Cl and CsADM-Cl. Viable cells were calculated at predetermined (24 h, 72 h  
6  
7 323 and 120 h) period by incubating the hydrogel coated coverslips with MTT (Merk Millipore,  
8  
9 324 Germany) solution and subsequently dissolving the formazan crystal by adding equivalent  
10 325 amount of dimethyl sulfoxide (DMSO). Subsequently, absorbance was taken at 570 nm,  
11  
12 326 experiments were repeated thrice, and mean was taken.  
13  
14  
15

#### 16 327 *2.12.2.2. Proliferation Assay*

17  
18  
19 328 Proliferating cell nuclear antigen (PCNA) antibody (BioLegend, USA) was used for  
20 329 immunofluorescent study (IF) of PCNA (Green) in proliferating HFCs on hydrogels. Hydrogel-  
21 330 coated coverslips were seeded with HFCs (15,000 cells/coverslip) and incubated for 5 days.  
22  
23 331 Post incubation, coverslips were fixed and permeabilized with ice-cold 70 % ethanol for 15  
24 332 minutes, followed by washing with PBS and blocking in BSA (1% in PBS) for 15 minutes at  
25 333 room temperature. Cells seeded hydrogels were stained with PCNA monoclonal antibody  
26 334 tagged with secondary for 1 h at room temperature and subsequently washed with PBS to  
27 335 remove background and imaged using inverted fluorescence microscope. Experiment was  
28  
29 336 repeated thrice to confirm reproducibility of data.  
30  
31  
32  
33  
34

#### 35 337 *2.12.2.3. Apoptosis Assay*

36  
37  
38 338 Apoptosis assay was executed using DeadEnd Fluorometric Terminal deoxynucleotidyl  
39 339 transferase dUTP nick end labeling (TUNEL) system (Promega, USA) following the  
40 340 manufacturer's guidelines. Briefly, hydrogel-coated coverslip were taken as sample and lysine  
41 341 coated coverslips served as control. HFC's were seeded (15,000 cells/coverslip) and cultivated  
42 342 for 5 days. Post 5 days of cultivation, samples were stained after processing and images were  
43 343 documented using ZEISS inverted fluorescence microscope.  
44  
45  
46  
47  
48

#### 49 344 *2.12.3. Cells encapsulation in pre-gel*

50  
51 345 For encapsulating HFCs in hydrogel, CCol-Cl and CsADM-Cl were processed in sterile  
52 346 parallel blinded fashion. Gels were fabricated in 24 well plates containing 2 mL pregel solution  
53 347 of each group with 1,00,000 HFCs/mL. After gelling, media was supplied to gels and media  
54 348 was changed every day to avoid cell death. The viability of HFCs in hydrogels was determined  
55 349 post 72 h using the Live/Dead kit (Invitrogen, USA), following manufactures protocol. Labeled  
56  
57  
58  
59  
60

1  
2  
3 350 cells were then micrographed under an inverted microscope, and images were captured using  
4  
5 351 the Zen software. Viable/Live cells were stained green (tagged with calcein AM), while dead  
6  
7 352 cells were stained red (tagged with EthD-1).

#### 9 353 *2.12.4. Quantification of hydrogels Contraction*

11  
12 354 CCol, CsADM, CCol-Cl and CsADM-Cl contraction after cells seeding/unseeded was  
13  
14 355 analysed using macroscopic image analysis (from two independent batches of ADM isolation).  
15  
16 356 Free-floating crosslinked, and uncrosslinked hydrogels were imaged after 12 h, 1, 3, and 7 days  
17  
18 357 in culture.

#### 19 358 *2.13. Host response of the CCol-Cl and CsADM-Cl in vivo*

21  
22 359 All *in vivo* experiments were executed under compliance of the Institutional Animal  
23  
24 360 Ethical Committee guidelines of the Indian Institute of Technology, Kharagpur, India. To  
25  
26 361 assess the host response *in vivo*, the subcutaneous injection of the CCol-Cl and CsADM-Cl in  
27  
28 362 dorsal region was performed in albino Wistar rat (150-200 kg; n=3 per group). Prior to  
29  
30 363 experiment, peritoneal injection of ketamine was performed to anesthetize the rats. Food and  
31  
32 364 water supply were provided freely to the rats post-surgery 12 h and light/dark cycle of 12 h  
33  
34 365 was maintained during the study. On day 14, the rats were sacrificed; CCol-Cl and CsADM-  
35  
36 366 Cl along with surrounding tissues were retrieved, followed by fixation in 4% paraformaldehyde  
37  
38 367 (PFA) and processed for H&E, TB, and Masson's Trichome (MT) staining. Major organs were  
39  
40 368 also harvested from rat on day 14 days to assess organ toxicity, and H&E was performed to  
41  
42 369 establish the biocompatibility of the hydrogels.

42 370

#### 43 371 *2.14. Full thickness wound healing in Burn model*

##### 44 372 *2.14.1. In vivo Burn model creation*

45  
46  
47  
48 373 For burn model, Wistar rat (150-200 g each) was taken and all *in vivo* experiments were  
49  
50 374 performed as per guidelines of the Institutional Animal Ethical Committee, Indian Institute of  
51  
52 375 Technology, Kharagpur, India. Rats were anesthetized by intraperitoneal injection of ketamine  
53  
54 376 hydrochloride; then dorsum was shaved to remove hair. The burn model was created as  
55  
56 377 previously reported.<sup>43</sup> Briefly, a custom-made 220 g aluminum rod with copper template of 1.5  
57  
58 378 cm diameter was heated in a 100 °C water bath for 5 min and placed on the posterior-dorsum  
59  
60 379 of each rat for 8 s. Subsequently, the rat was resuscitated by intraperitoneal injection of saline

1  
2  
3 380 within 1 h post burning. To follow the current clinically accepted treatment, burn wound  
4 381 excisions were executed 48 h post burn injury. The FT skin was removed to generate a 2 cm  
5 382 diameter circular wound; CCol-Cl/CsADM-Cl pregel were injected at the wound site, and  
6 383 Tegaderm™ dressing (3M Science Applied to Life™, USA) was applied to hydrogels on the  
7 384 wound bed. SHAM wounds were only covered with Tegaderm™ dressing. For the study, 3 rats  
8 385 were taken for each group and for each period.

386

#### 17 387 *2.14.2. Histomorphometric Analysis*

19  
20 388 Hydrogel explants were collected at day 7, 14, and 21; fixed using 4% PFA. Following  
21 389 fixation, tissues were dehydrated in ethanol graded series (70% to 100%), embedded in paraffin  
22 390 to form block, sectioned using a microtome (3 μm thickness), and stained with H&E. Section  
23 391 images were processed using ImageJ (version 6) for quantification of reepithelialisation,  
24 392 wound distance, granulation area, newly formed appendages and thickness of the newly formed  
25 393 epithelium. Masson's Trichome (MT) staining was performed for analysis of collagen  
26 394 morphology and intensity. Sections were also stained with anti-CD31 and anti-CK10 for  
27 395 confirmation of blood vessels and reepithelialisation in different groups.

#### 34 396 *2.15. Gene expression (RT-PCR analysis)*

35  
36  
37 397 Regenerated tissues were retrieved on day 21 from each group and TRIzol Reagent  
38 398 (Thermo Scientific, USA) was used for isolation of total RNA following the manufacturer's  
39 399 instructions. RNA quality was determined using NanoDrop™ (NanoDrop™ 2000/2000c,  
40 400 Thermo, USA) (high quality RNA has OD 260/280 nm ratio between 1.8 and 2.0) and  
41 401 equivalent RNA of each group were reverse transcribed to cDNA using the cDNA Synthesis  
42 402 kit (Thermo Scientific, USA), following the manufacturer's protocol. The primer sequences  
43 403 used for the study are given in **supporting information**.

#### 49 404 *2.16. Statistics*

50  
51  
52 405 GraphPad Prism software (version 5.02, La Jolla, CA, USA) was used to execute  
53 406 statistical evaluations of data obtained from different groups. All experiments were repeated  
54 407 thrice unless mentioned, and the data signifies mean ± SD. The level of significance was  
55 408 determined as  $P < 0.05$ .

### 3. Results

Hybrid hydrogels (CCol, CCol-Cl, CsADM, and CsADM-Cl) were fabricated successfully at physiological pH and temperature using CTS, DHF-I and ADM/Col. The possible mechanism of hydrogel formation with ADM/Col and cross-linking reaction by CTS and DHF-I is shown in **Schematics 1**. Interestingly, both CCol-Cl and CsADM-Cl were observed to be injectable using syringe with 18 G needle. Uncrosslinked hydrogel took  $15 \pm 2$  min for gelation, while crosslinked hydrogels gelled within  $5 \pm 1$  min at  $37^\circ\text{C}$ .

#### 3.1. Extraction of sADM and Col

ADM was successfully prepared from rat dermis by a combinatorial treatment of Trypsin and Triton<sup>TM</sup> X-100. After decellularization, NS turned milky white from pinkish red, which represents the removal of cells. The efficiency of the, decellularization process was confirmed using H&E, Col I, AB, and DAPI staining. ADM, in contrast to NS, showed the absence of any cell nucleus as observed by H&E and DAPI staining, whereas major protein Col and GAGs had similar intensity in both NS and ADM sections as shown by Col I and AB staining, respectively (**Figure 1a**). SDS-PAGE (**Figure 1b**) shows existence of a mixture of proteins/peptides in ADM as evident from the presence of different molecular weights bands, especially bands at lower molecular weight. Such observation signifies the preservation of bioactive molecules in ADM, post-decellularization. The absence of DNA fragment in ADM was demonstrated by the GelDoc image (**Figure 1c**), which corroborates with the findings of H&E and DAPI staining. NS and ADM were processed to isolate and to quantify DNA. In comparison to NS ( $1121 \pm 210$  ng/mg dry weight), ADM showed significantly reduced ( $p < 0.001$ ) DNA content ( $30.14 \pm 12.34$  ng/mg dry weight), as observed in **Figure 1d**. Further, Col content of NS and ADM did not show any significant difference; Col content in ADM was  $60.12 \pm 5.31$  % of dried tissue whereas in NS it was  $52.31 \pm 4.61$  % of dried tissue (**Figure 1d**). Also, sGAG content was not observed to vary significantly in the ADM ( $0.44 \pm 0.06$  % dry weight), when compared to NS ( $0.512 \pm 0.07$  %) (**Figure 1d**). The presence of essential growth factors (BMP-2, VEGF and TGF- $\beta$ ) was revealed through ELISA assay in both NS and ADM (**Figure S1a**).

Isolated rat tail Col was characterized using SDS PAGE. Rat tail Col demonstrated classic band pattern for type I Col i.e. doublet at molecular weight  $\sim 215$  and  $\sim 235$  kDa; also, an additional doublet at  $\sim 115$  and  $\sim 130$  kDa in SDS page (**Figure S1b**).



### 3.2. DHF-I Synthesis

Iodine reacts with double bond of DHF via electrophilic addition reaction and formed DHF-I which was confirmed through  $^1\text{H}$  NMR analysis of pristine DHF and DHF-I. In the  $^1\text{H}$  NMR (**Figure S2a**) spectrum of DHF, the chemical shifts between  $\delta = 3.49\text{--}3.52$  ppm signify methoxy proton (H1) of cis and trans isomers. The chemical shifts between  $\delta = 6.27\text{--}6.29$  ppm are because of H2 protons. The chemical shifts at  $\delta = 5.78$  and  $6.07$  ppm are due to the presence of unsaturated protons (H3). The disappearance of chemical shift at  $\delta = 5.78$  ppm, while appearance of new chemical shift between  $\delta = 3.78\text{--}3.82$  ppm in the NMR spectrum of iodinated product reveal the successful formation of DHF-I from DHF through iodination reaction.

### 3.3. Macroscopic appearance of hydrogel

Uncrosslinked hydrogels (CCol/CsADM) were softer with round edges in comparison to crosslinked hydrogels (CCol-Cl/CsADM-Cl), which were observed to be rigid structures with defined edges and easy to handle with the help of tweezers (**Figure 2a-d**). SEM analysis of hydrogel microstructure revealed nano-fibrillar morphology in both the group i.e. CCol (**Figure 2e**) and CsADM (**Figure 2g**). Further, crosslinking of hydrogels did not affect adversely intrinsic property of the self-assembly into nano-fibrillar structure and the similar structure was observed in CCol-Cl (**Figure 2f**), and CsADM-Cl (**Figure 2h**). After crosslinking, fiber diameter was reduced marginally; fiber diameter of CCol, CCol-Cl, CsADM and CsADM-Cl hydrogel were  $\sim 110$  nm,  $\sim 105$  nm,  $\sim 135$  nm, and  $\sim 95$  nm, respectively (**Figure 2i-l**). The presence of iodine in crosslinked matrix was confirmed by EDAX scanning; both crosslinked hydrogel variants CCol-Cl (**Figure 2m and n**) and CsADM-Cl (**Figure 2o and p**) showed uniform iodine distribution.

### 3.4. Hydrogel ICC

For evaluating the presence of characteristic ECM biomolecules such as Col I and Fibronectin, ICC was performed against specific antibody (**Figure S3**). The distribution of ECM active biomolecules was similar in NS and ADM. Also, cytokines and growth factors that are vital for dermal neovascularization and regeneration, like TGF- $\beta$ , VEGFA, MCP-1, IL-8, were also evaluated in the NS, ADM, CsADM and CsADM-Cl hydrogel. The ICC results revealed the fact that although intensity of the ICC stains diminished, yet part of each growth

1  
2  
3 470 factor was preserved in the crosslinked hydrogel (**Figure S3**). Altogether, native nanofibrillar  
4 471 structure and bioactive components were well preserved after crosslinking with CTS and DHF.

### 7 472 3.5. Rheological characterization of Hydrogel

10 473 The rheological properties of hybrid hydrogel were studied using parallel plate  
11 474 rheometer (**Figure 2q-u**). Average viscosity at 25 °C of pre-gel solution was 1.5 Pa. s and 1.9  
12 475 Pa. s for CCol and CsADM, respectively. Storage modulus ( $G'$ ) and loss Modulus ( $G''$ )  
13 476 increases with an increase in temperature from 15 to 37 °C (**Figure 2q and r**).  $G'$  value was  
14 477 higher than  $G''$  for both the variants by factor of  $\sim 5$ , which denotes the solid-like behavior of  
15 478 pre-gel solutions after gelation. The steady state  $G'$  after complete gelation varied non-linearly  
16 479 with temperature/time and when compared to uncrosslinked variant, crosslinked variant  
17 480 showed higher  $G'$  (**Figure 2s**). After gelation, frequency response was studied and the value of  
18 481  $G'$  was independent of frequency (**Figure 2 t and u**) indicating the frequency independent  
19 482 gelation behavior. At all frequencies, crosslinked hydrogel showed higher  $G'$  when compared  
20 483 to uncrosslinked variant, representing superior stability and strength.

### 29 484 3.6. FTIR

32 485 FTIR spectra of CCol, CCol-Cl, CsADM, and CsADM-Cl are shown in **Figure S2b**.  
33 486 The CCol hydrogel (**Figure S2b-A**) showed peaks at 3357, 2982, 1640, 1578, and 1414  $\text{cm}^{-1}$   
34 487 which are responsible for frequencies of N-H bond stretching (amide A), C-H stretching,  
35 488 amide-I stretching, amide-II stretching, and amide III stretching, respectively. The crosslinked  
36 489 hydrogel (**Figure S2b-B**), CCol-Cl exhibited peaks for amide A, C-H stretching, amide I,  
37 490 amide II and amide III at 3340, 2972, 1634, 1556, and 1405  $\text{cm}^{-1}$ , respectively. While, CsADM  
38 491 hydrogel (**Figure S2b-C**) demonstrated peaks of N-H stretching, C-H stretching, amide I,  
39 492 amide II and amide III at 3366, 2982, 1633, 1567 and 1414  $\text{cm}^{-1}$ , respectively. The crosslinked  
40 493 hydrogel (**Figure S2b-D**), CsADM-Cl illustrated peaks for amide A, C-H stretching, amide I,  
41 494 amide II and amide III stretching frequencies at 3325, 2982, 1634, 1556, and 1409  $\text{cm}^{-1}$ ,  
42 495 respectively. Further, the increasing of peak intensity at 1634  $\text{cm}^{-1}$  for both crosslinked  
43 496 hydrogel (**Figure S2b-B and D**) implies the formation of Schiff base by the chemical  
44 497 crosslinking between chitosan, collagen/sADM and iodinated DHF via imine ( $\text{C}=\text{N}$ ) bond [38].

45 498 Triple helix integrity of Col fibers in both isolated Col and ADM is a critical factor  
46 499 attributing to good combination of mechanical and biological properties.<sup>44</sup> This further will  
47 500 dictate the hydrogels behavior, *in vivo*. The ratio of the O.D. 1235  $\text{cm}^{-1}$  and O.D. 1450  $\text{cm}^{-1}$  can  
48 501 assess Col's triple helix integrity. Also, values around 0.5 have been reported for denatured,

1  
2  
3 502 while those around 1 indicate native triple helix structures.<sup>45,46</sup> In case of the blend samples  
4 503 (CCol and CsADM), the value obtained was 1.01 and 1.00, respectively. Similarly, the values  
5 504 obtained were 1.03 and 1.04 for crosslinked samples CCol-Cl and CsADM-Cl respectively.  
6  
7 505 Such observations indicate that the crosslinking did not destabilize the triple helix structure.  
8  
9 506 Absence of band at 1706  $\text{cm}^{-1}$  (corresponding to free acetic acid)<sup>45</sup> in any of the groups  
10 507 evidences complete neutralization of the hydrogels, which is essential for imparting bioactive  
11  
12 508 biocompatible surface *in situ* for neighboring cells infiltration and proliferation.

### 16 509 3.7. Iodine release kinetics

18  
19 510 **Figure S4** demonstrates the iodine releasing curves of the CsADM-Cl hybrid hydrogel  
20 511 in PBS and buffered enzymatic solution at different predetermined period. Iodine release rate  
21 512 from hydrogel was slower in PBS, when compared to enzymatic solution. There was an initial  
22 513 rapid release (in PBS:  $1919.84 \pm 105.9$  ppm; in enzyme:  $3771.51 \pm 163.4$  ppm) in 6 h of  
23 514 incubation. Further, the CsADM-Cl hydrogel showed a prolonged release behavior of iodine  
24 515 (in PBS:  $2190.67 \pm 106.5$  ppm; in enzyme:  $3959.35 \pm 191.23$  ppm) till 24 h, after which it  
25 516 attained the plateau phase.

### 31 517 3.8. Antioxidant Assay

33  
34 518 Antioxidant molecules have been reported to exert positive effect on wound healing  
35 519 progression and pace by regulating burden of excess ROS in wound site.<sup>47</sup> Thus, iodine  
36 520 introduction in the hydrogel matrix plays another vital role, since iodine has antioxidant  
37 521 activity.<sup>48</sup> Antioxidant potential was evaluated by measuring the efficiency of hydrogels to  
38 522 scavenge DPPH. All hydrogels showed differential reduction in DPPH peak, which was  
39 523 attributed to hydrogen atom donation or electron transfer from parent molecule to DPPH free  
40 524 radical. DPPH scavenging efficiency of CCol, CsADM, CCol-Cl and CsADM-Cl was  $19.54 \pm$   
41 525  $0.9$ ,  $24.14 \pm 2.12$ ,  $58.60 \pm 5.21$  and  $63.20 \pm 6.21$  %, respectively (**Figure S2c**). These results  
42 526 demonstrated that crosslinked variants had significantly ( $p < 0.001$ ) superior antioxidant  
43 527 potential, when compared to uncrosslinked variants. Also, hybrid hydrogels can prevent cell  
44 528 damage and enhance viability by reducing excess ROS *in vitro*.

### 54 529 3.9. Haemocompatibility

56 530 Blood compatibility of skin substitute is important because it would stimulate the blood  
57 531 defense systems (i.e. coagulation or fibrinolysis) which can further worsen the situation.<sup>49</sup>  
58 532 Haemocompatibility is especially essential for FT/critical burn wounds with significant loss of

1  
2  
3 533 skin components (either epidermis or epidermis dermis both), and hence, bringing skin  
4 534 substitute in direct contact to different body fluids. The percentage haemolysis is a direct  
5 535 indicator of the extent of erythrocytes damage, when exposed to sample of interest. CCol-Cl,  
6 536 CsADM-Cl, positive control (Triton™ X-100) and negative control (saline) on direct contact  
7 537 with RBCs showed absorbance of  $0.047 \pm 0.02$ ,  $0.048 \pm 0.01$ ,  $0.6835 \pm 0.02$  and  $0.038 \pm 0.01$ ,  
8 538 respectively. The percentage haemolysis due to CCol-Cl/CsADM-Cl was  $1.39 \pm 0.12$  % and  
9 539  $1.55 \pm 0.13$  %. Generally, haemolysis <5% is acceptable for suitable biomaterial to be used *in*  
10 540 *vivo*. Higher percentage of hemolysis reveals biomaterial's poor haemocompatibility. All  
11 541 materials used clinically in current practice, including PVC, meet these guidelines.<sup>50</sup> The data  
12 542 suggested that CCol-Cl and CsADM-Cl can exhibit clinically desired haemocompatibility.

### 21 543 3.10. Antibacterial assay

22  
23  
24 544 Burn wounds are prone to bacterial infection.<sup>51</sup> Therefore, dressings with the inherent  
25 545 antibacterial property will be beneficial to remove the bacterial load and inflammatory response  
26 546 from the wounds. Iodine is reported to exhibit significant antibacterial property even at 1  
27 547 ppm.<sup>51,52</sup> For demonstrating antibacterial activity, hydrogels were challenged with two  
28 548 pathogens (*E. coli* and *S. aureus*) at a concentration of about  $10^6$  CFU and the cell-count  
29 549 reductions after 2h treatment were recorded post incubation for 12 h in agar gel. **Figure 3a-d**  
30 550 shows the antibacterial activity of the hydrogel. The CCol and CsADM exhibited good activity  
31 551 against gram positive and gram-negative bacteria. CCol and CsADM showed log reduction of  
32 552  $7.72 \pm 4.2$  and  $7.89 \pm 3.5$  against *E. coli*, respectively; whereas  $8.39 \pm 5.2$  and  $8.55 \pm 3.4$  against  
33 553 *S. aureus*, respectively (**Figure 3b**). Control group displayed development of lawn post direct  
34 554 plating (**Figure 3a**). For calculating log reduction, CFU from  $10^5$  dilution (**Figure 3d**) in  
35 555 control was utilized. On other hand, all DHF-I crosslinked hydrogel, i.e., CCol-Cl and CsADM-  
36 556 Cl demonstrated outstanding antibacterial property (**Figure 3a**). No survival colony was  
37 557 observed after incubation for 12 h in agar gel. Further, Live/Dead assay also revealed the  
38 558 presence of red stained cells denoting non-viable bacterial cells on hydrogel surface (**Figure**  
39 559 **3c**).

### 52 560 3.11. CAM Assay

53  
54  
55 561 Capillary formation on CAM was observed to investigate the angiogenesis potential of  
56 562 CCol-Cl and CsADM-Cl hydrogels (**Figure 3e and f**). After incubation with CCol-  
57 563 Cl/CsADM-Cl disc for 3 days, the embryo was live, indicating the non-toxic nature of  
58 564 hydrogel. Further, the blood vessels were also found to be branched therein. Interestingly, after

1  
2  
3 565 72 h of incubation, there were significantly ( $p < 0.001$ ) higher number of blood vessels  
4 566 approaching toward the CsADM-Cl hydrogel ( $50 \pm 3$ ), when compared to CCol-Cl ( $21 \pm 2$ )  
5 567 hydrogel on treated CAM. Moreover, CsADM-Cl treated CAM led to a higher number of  
6 568 branch points, when compared to CCol-Cl treated CAM.  
7  
8  
9

### 10 569 3.12. *In vitro* Assays

#### 11 570 3.12.1. *Indirect Assay*

12  
13  
14  
15 571 To evaluate the toxicity of the eluted remnant material hydrogels conditioning media,  
16 572 treated cells were stained using Rhodamine phalloidin/DAPI. HFC & HKC showed similar  
17 573 morphology in conditioned medium like control after 72 h of incubation (**Figure 4a**). HFC's  
18 574 treated with CsADM-Cl conditioning media displayed well-spread cytoskeleton and extended  
19 575 F-actin filaments, revealing higher cell-to-cell contact.  
20  
21  
22  
23

24 576 *In vitro*, wound healing or scratch assay was also performed to evaluate the effect of  
25 577 conditioning media on proliferation potential of HFC's. Interestingly, none of the group  
26 578 showed an adverse effect on the proliferation rate of HFC's when treated for 24 h.  
27 579 Wounds/scratch treated with CCol-Cl/CsADM-Cl conditioning media showed the significantly  
28 580 ( $p < 0.01$ ) higher rate of migration of HFC's in the denuded path after 6 h of treatment (**Figure**  
29 581 **4 b and d**). After 12 h of treatment, CsADM-Cl treated group showed complete wound  
30 582 coverage (100 %) in comparison to control ( $68.675 \pm 5.61$  %) and CCol-Cl ( $80.52 \pm 6.21$ %).  
31 583 Similarly, in the case of HKC's, they were observed to follow the increasing trend of migration  
32 584 with time. Significantly higher migration rate ( $p < 0.001$ ) of HKC's was supported by  
33 585 conditioning media of CCol-Cl/CsADM-Cl, as observed in **Figure 4c and e**. After 24 h of  
34 586 treatment, CsADM-Cl conditioning media treated group showed wound closure of  $93.12 \pm$   
35 587  $2.11$  % in comparison to control of  $33.56 \pm 1.24$  % and CCol-Cl conditioning media treated a  
36 588 group of  $64.00 \pm 3.44$  % ( $p < 0.001$ ).  
37  
38  
39  
40  
41  
42  
43  
44  
45  
46

#### 47 589 3.12.2. *Direct Assay*

48  
49  
50 590 HFC's were directly plated on hydrogel-coated coverslips; subjected to MTT assay to  
51 591 assess metabolic activity, proliferation assay (PCNA) to identify actively proliferating cells  
52 592 and apoptosis staining to identify apoptotic cells. Both HFC and HKC showed an increasing  
53 593 growth trend of metabolically active cells with time, revealing the non-toxic behavior of the  
54 594 CCol-Cl/CsADM-Cl. The proliferation rate of cells was significantly ( $p > 0.05$ ) higher in  
55 595 CsADM-Cl treated group, when compared to CCol-Cl (**Figure S5a and b**). After 5 days of  
56 596 cultivation, there were a significantly ( $p > 0.001$ ) higher number of PCNA positive cells (**Figure**

1  
2  
3 597 **5a and b**) in CsADM-Cl ( $210 \pm 15$ ), when compared to CCol-Cl ( $142 \pm 8$ ). Also, cells  
4  
5 598 cultivated on CCol-Cl showed significantly ( $p > 0.001$ ) higher number of PCNA positive cells  
6  
7 599 when compared to Control. Further, there were no apoptotic cells in any of the group (**Figure**  
8  
9 600 **S5c**) demonstrating the excellent cellular compatibility of the hydrogel.

### 10 11 601 *3.12.3. HFC Encapsulation in hydrogel*

12  
13 602 **Figure 5 c, d and s6** represent the cells encapsulated into hydrogels. It is noticeably  
14  
15 603 demonstrated that the majority of cells were live, depicting green fluorescence post 72 h of  
16  
17 604 incubation in hydrogels, suggesting the dual crosslinked nanofibrillar microenvironment were  
18  
19 605 non-toxic to the HFC's.

### 20 21 606 *3.12.4. ECM hydrogel contraction*

22  
23  
24 607 Hydrogel showed an increased contraction, when incubated from 12 h to 7 days in  
25  
26 608 culture. Also contraction rate relied on the crosslinking status of the hydrogel (**Figure 5 e and**  
27  
28 609 **f**). The unseeded hydrogel area remained same regardless of being crosslinked/  
29  
30 610 uncrosslinked/left for different time point (data not shown). Hydrogel contraction (**Figure 5f**)  
31  
32 611 in CsADM-Cl ( $81.88 \pm 3.1 \%$ ) and CCol-Cl ( $76.35 \pm 6.5 \%$ ) hydrogel groups were significantly  
33  
34 612 lesser, when compared to CCol ( $42.35 \pm 5.89 \%$ ) and CsADM ( $47.35 \pm 3.2\%$ ) groups.  
35  
36 613 Crosslinking imparted stability to hydrogel networks. Hence, crosslinked hydrogels were  
37  
38 614 observed to contract lesser, when compared to uncrosslinked hydrogels.

### 39 615 *3.13. Host response to the hydrogel*

40  
41 616 To evaluate host response to hydrogel, CCol-Cl/CsADM-Cl was injected  
42  
43 617 subcutaneously in the rat. The treated groups were observed to be healthy, and there were no  
44  
45 618 mortality during the study. The rat weight did not vary abruptly during the study period (data  
46  
47 619 not shown). After 2 weeks of injection, CCol-Cl/CsADM-Cl was retrieved along with  
48  
49 620 surrounding tissue and was subjected to histological staining for studying the interaction  
50  
51 621 between the hydrogel and the host tissue, as shown in **Figure 6a and b**. H&E staining  
52  
53 622 demonstrated host tissue integration with CCol-Cl/CsADM-Cl and also host cell infiltration in  
54  
55 623 hydrogel was evident. Interestingly, as displayed in **Figure 6b**, CsADM-Cl showed more  
56  
57 624 infiltration and proliferation of cells, as compared to CCol-Cl.

58  
59 625 MT staining of the retrieved hydrogels showed absence of capsular layer/fibrosis and  
60  
61 626 the presence of blood vessels in the interface area. Further, the interfacial layer was also  
62  
63 627 characterized by the presence of dense collagen fiber deposition, demonstrating stimulated cell

1  
2  
3 628 infiltration in CCol-Cl/CsADM-Cl. To assess inflammatory response to hydrogel, TB staining  
4 629 was performed. TB staining revealed very few mast cells near the implanted zone, and also,  
5 630 there were no mast cells infiltration inside the CCol-Cl/CsADM-Cl. This minimal  
6 631 inflammatory response after CCol-Cl/CsADM-Cl injection is similar to normal wound healing  
7 632 cascade. These findings establish the biocompatible nature of CCol-Cl and CsADM-Cl and  
8 633 also demonstrate that neither of hydrogel triggered an adverse immune response, *in vivo*.

9  
10  
11  
12  
13 634 Plausible toxicity of CCol-Cl/CsADM-Cl to vital organs was also determined by  
14 635 retrieving major organs after two-week post-injection. Major organs (liver, kidney, lung, and  
15 636 heart) retrieved were analyzed *via* histological staining, and there were no significant necrosis  
16 637 or pathological changes in the anatomy of the organs of the CCol-Cl/CsADM-Cl treated group  
17 638 in comparison to untreated group (**Figure S7**). Cardiac muscles in the heart had the similar  
18 639 anatomy for all groups, and also there was the absence of any sign of fibrosis or inflammation.  
19 640 Hepatocytes distribution in the liver of treatment groups showed the normal anatomy. Also,  
20 641 Lungs had no signs of fibrosis in treatment groups. Moreover, in kidney sections, glomerulus  
21 642 structure was distinctly visible for all groups. These results signify that CCol-Cl and CsADM-  
22 643 Cl did not exert any toxic effect on major organs in rat model.

#### 31 644 *3.14. Hydrogel treatment of dorsal burn injury model*

32  
33  
34 645 Burn model was prepared as demonstrated in **Figure S8**; FT wounds created post burn  
35 646 injury, were treated with crosslinked hybrid hydrogels CCol-Cl/CsADM-Cl; whereas  
36 647 Tegaderm™ covered wounds were marked as SHAM group, which served as control for the  
37 648 study. Tegaderm™ was also placed on top of hydrogels to secure their position on the wound  
38 649 bed. Animals were sacrificed after predetermined period i.e. 7, 14 and 21 days post-treatment  
39 650 for histological analysis. Optical images revealing morphological changes in wound closure  
40 651 for various groups are provided in **Figure 6c and d**. Wound treated with CsADM-Cl showed  
41 652 significantly enhanced wound closure (~ 89.23 % healing) 7 days post-surgery, when compared  
42 653 to groups treated with CCol-Cl (~ 78.21 % healing)/SHAM (~ 65.11 % healing) (**Figure 6d**).

43  
44  
45 654 By day 14, ~ 90.21% and ~ 95.40 % of the wounded area was reepithelialised in wounds  
46 655 treated with CCol-Cl and CsADM-Cl, respectively. This was significantly higher than the  
47 656 SHAM group (~ 75.52 %). 21 days post-surgery CsADM-Cl treated groups showed complete  
48 657 wound closure i.e. ~ 99.12 %, while CCol-Cl/SHAM groups were still in the healing phase.  
49 658 However, CCol-Cl (~ 97.254 %) treated groups showed significantly higher % healing, when  
50 659 compared to the SHAM group (~ 88.62) on day 21 (**Figure 6d**). All these findings suggest that  
51  
52  
53  
54  
55  
56  
57  
58  
59  
60

1  
2  
3 660 the wound treated with CsADM-Cl showed enhanced wound closure; hence, better-wound  
4  
5 661 healing as compared to CCol-Cl/SHAM groups.  
6  
7  
8  
9

662

### 10 663 *3.15 Histomorphometric Analysis*

11  
12 664 Wound healing is a multifaceted repair process involving recruitment of cells to the  
13 665 wound area by releasing chemoattractants, followed by cells proliferation and differentiation.  
14 666 These pathobiological processes lead to the formation of new tissue; hence, wound closure. To  
15 667 further analyze the healing progression in different groups, H&E staining was performed to  
16 668 detail the morphological changes in different layers of skin (**Figure 7**). At day 7 post surgery,  
17 669 the length of wound reduced significantly in wounds treated with CsADM-Cl ( $0.56 \pm 0.09$  cm)  
18 670 and CCol-Cl ( $1.08 \pm 0.12$  cm), when compared to SHAM group ( $1.36 \pm 0.14$  cm). In addition,  
19 671 CsADM-Cl treated wounds demonstrated significantly enhanced reepithelialisation ( $13.49 \pm$   
20 672  $1.2$  cm) accompanied with lower area of granulation ( $31.26 \pm 2.05$  mm<sup>2</sup>). This was  
21 673 characterized with thicker and well-organized granulation tissue, when compared to CCol-Cl  
22 674 (reepithelialisation  $9.74 \pm 0.85$  cm and Granulation area  $42.69 \pm 2.87$  mm<sup>2</sup>)/SHAM treated  
23 675 group (reepithelialisation  $7.46 \pm 0.65$  cm and Granulation area  $74.97 \pm 5.21$  mm<sup>2</sup>) (**Figure 7b,**  
24 676 **c & d**). Granulation tissue formation is an essential aspect of wound repair and regeneration.  
25 677 The granular tissue is composed of synthesized ECM, fibroblasts, and bioactive molecules,  
26 678 dictating the different phases of healing [52-56]. By day 14, the length of wounds (Control:  
27 679  $0.9307 \pm 0.11$  cm, CCol-Cl:  $0.7026 \pm 0.1$  cm, CsADM-Cl:  $0.3187 \pm 0.05$  cm) and granulation  
28 680 area (Control:  $38.447 \pm 4.21$  mm<sup>2</sup>, CCol-Cl:  $28.293 \pm 1.92$  mm<sup>2</sup>, CsADM-Cl:  $18.368$  mm<sup>2</sup>)  
29 681 further decreased, whereas the length of reepithelization (Control:  $11.578 \pm 0.98$  cm, CCol-Cl:  
30 682  $14.189 \pm 1.18$  cm, CsADM-Cl:  $16.749 \pm 1.48$  cm) increased; indicating healing progression in  
31 683 all the groups (**Figure 7b, c & d**).

32 684 At 21 Days post-surgery, no wound was observed in groups treated with CsADM-Cl  
33 685 whereas CCol-Cl and Control treated group showed wound length of  $0.514 \pm 0.09$  cm and  $0.319$   
34 686  $\pm 0.08$  cm, respectively (**Figure 7b**). CsADM-Cl treated group exhibited complete  
35 687 reepithelization with defined epidermal-dermal junction, when compared to CCol-Cl/Control  
36 688 group. The epidermal-dermal junction forms a surging interdigitating interface (inset of **Figure**  
37 689 **7**), which increases surface area; hence, strengthening the contact between the dermis and  
38 690 epidermis. Also, CsADM-Cl treated group exhibited a significantly higher number of newly  
39 691 formed appendages ( $40 \pm 5$ ), when compared to CCol-Cl ( $12 \pm 2$ )/Control ( $4 \pm 2$ ) treated group



1  
2  
3 692 (Figure 7f). Newly formed appendages in wound area signify a better quality of wound  
4  
5 693 healing. Additionally, we also measured the thickness of epithelium post 21 days of surgery.  
6  
7 694 The epidermis thickness of the Control, CCol-Cl, and CsADM-Cl treated group was  $97 \pm 8.21$   
8  
9 695  $\mu\text{m}$ ,  $84 \pm 10.1 \mu\text{m}$  and  $59 \pm 3.24 \mu\text{m}$ , respectively (Figure 7e). The epidermal thickness of  
10  
11 696 CsADM treated group was much closer to reported values of the epidermal thickness of NS,  
12  
13 697 i.e.  $42.0 \pm 7.1 \mu\text{m}$  [57].

14 698 As shown in Figure 8a, collagen deposition and arrangement were visualized and  
15  
16 699 analyzed using MT staining 21 days post-wounding. Augmented deposition of collagen was  
17  
18 700 observed in CCol-Cl, and CsADM-Cl treated groups, when compared to the SHAM group.  
19  
20 701 However, collagen deposition in the dermis was more organized with basket weave pattern in  
21  
22 702 the CsADM-Cl treated group. Also, densely packed random collagen fibers were observed in  
23  
24 703 CCol-Cl treated group and SHAM group exhibited partial dysplastic collagen fibers.  
25  
26 704 Quantitative image analysis of MT stained sections revealed collagen index (intensity of  
27  
28 705 Collagen deposition) of  $0.42 \pm 0.02$ ,  $0.74 \pm 0.06$  and  $0.639 \pm 0.04$  for SHAM, CCol-Cl, and  
29  
30 706 CsADM-Cl, respectively (Figure 8a and b). Collagen Index of CsADM-Cl was closest to  
31  
32 707 Collagen Index of NS, as reported earlier (i.e.  $0.601 \pm 0.038$ ) [57].

33 708 In wound healing, dermal regeneration, reepithelialisation and formation of secondary  
34  
35 709 structure play a pivotal role to restore tissue functionality, strength, and aesthetic view.<sup>58</sup> It has  
36  
37 710 been widely reported that cytokines and growth factors are essential for accelerating wound  
38  
39 711 healing, regarding enhanced wound closure and reepithelialisation.<sup>59,60</sup> Therefore, accelerated  
40  
41 712 healing in CsADM-Cl treated group can be attributed to embedded native proteins, GAGs,  
42  
43 713 cytokines, growth factors and also to the unique antibacterial and ROS scavenging activity of  
44  
45 714 the hydrogel variant.

### 46 715 3.16. Immuno Histochemical Analysis

47 716 Angiogenesis is a fundamental necessity for rapid wound closure, especially in the case  
48  
49 717 of chronic wounds as blood vessels increase the inflow of oxygen and nutrients to the wound  
50  
51 718 area; henceforth, promote healing therein [61,63]. In the present study, angiogenesis through  
52  
53 719 *in vivo* model was assessed *via* CD31 immunofluorescence staining, as shown in Figure 8c  
54  
55 720 and d. Compared to SHAM, CCol-Cl treated group showed significantly ( $p < 0.05$ ) higher  
56  
57 721 number of blood vessels at day 7. Further, newly formed vessels were distinctly visible on more  
58  
59 722 organized granulation tissue of CsADM-Cl treated group. The angiogenesis induced was  
60  
723 significantly higher ( $p < 0.001$ ), when compared to both SHAM, and CCol-Cl treated group post  
724 7-days of surgery. The higher angiogenic activity of CsADM-Cl may be attributed to the

1  
2  
3 725 release of bioactive molecules from the hydrogel, *in situ*. At day 14, blood vessels were  
4 726 observed to follow an increasing trend in control treated group. In contrast, both CCol-Cl and  
5 727 CsADM-Cl treated group showed a decrease in number of vessels. The reason may be the rapid  
6 728 closure of wounds in CCol-Cl and CsADM-Cl treated group. Hence, requirements of blood  
7 729 vessels for the transport of nutrients and oxygen is less, whereas in SHAM group healing is  
8 730 still in progress.

9  
10  
11  
12  
13 731 Further, to demonstrate reepithelialisation and epidermal differentiation, CK 10  
14 732 antibody was used for staining 14- and 21-days post-surgery sections (**Figure 8e**). By day 14,  
15 733 no distinct expression of CK 10 was observed in both SHAM and CCol-Cl treated groups,  
16 734 revealing the absence of neopithelium in the wound area. Surprisingly, CsADM-Cl treated  
17 735 group revealed little CK-10 expression in thick epithelial layer, developing at the interface of  
18 736 the wound. At 21-day post-wounding, CsADM-Cl treated group showed clear, intense  
19 737 expression of CK-10 in the epithelial layer, revealing complete regeneration and resembling  
20 738 the NS tissue architecture. However, CCol-Cl treated group showed thick epithelium and  
21 739 expression of CK-10 was mild comparatively, while in control treated group, expression of  
22 740 CK-10 was non-specific.

### 31 741 3.17. RT-PCR Analysis

32  
33  
34 742 To evaluate the molecular aspect of healing in different groups, the expression of genes  
35 743 associated with skin wound healing (COL I, COL III, KRT 10, KRT 14) was assessed, 21 days  
36 744 post-wounding. As shown in **Figure 6e and f**, there was upregulation in Col I expression in  
37 745 CsADM-Cl treated group, when compared to both the SHAM/CCol-Cl treated group. This  
38 746 enhanced expression can be credited to accelerated wound healing observed in CsADM-Cl  
39 747 treated group. Interestingly, the downregulation in expression of Col III, KRT 10 and KRT 14  
40 748 in CsADM-Cl treated group, when compared to other group reveals that the reepithelialisation  
41 749 process was more complete and the remodeling phase has started to regain the tissue native  
42 750 strength.

## 50 751 4. Discussion

51  
52  
53 752 Bioactive matrices with appropriate physiochemical and biological properties are  
54 753 required to induce rapid wound closure, to support cell infiltration, adhesion and differentiation  
55 754 to regain tissue morphology and function. It has been established in the literature that burn  
56 755 wounds, if heal within 21 days, exhibit minimal scar formation.<sup>64</sup> In the present work, rapid  
57  
58  
59  
60

1  
2  
3 756 injectable bioactive hydrogel was developed by dual cross-linking of the sADM. The  
4  
5 757 compositional training allows the hydrogels to preserve inherent biochemical composition and  
6  
7 758 also lending the gel unique antioxidant and antibacterial property. Although sADM from varied  
8  
9 759 origin have been utilized either alone or as a hybrid for tissue engineering, but minimal reports  
10  
11 760 are available for an antibacterial sADM based hydrogel with retained bioactive cues. Our study  
12  
13 761 has utilized DHF-I as a crosslinker for the development of injectable sADM based hydrogel  
14  
15 762 with inherent antibacterial property for application in critical burn wounds. Perhaps this is the  
16  
17 763 first report for utilization of DHF-I crosslinker for wound healing study.

17 764 In our processing approach, ADM was decellularized using a combinatorial approach  
18  
19 765 and to lessen surgical trauma due to scaffold implantation in particular, injectable hydrogel of  
20  
21 766 decellularized tissue was developed using enzymatic (pepsin) digestion, as reported in the  
22  
23 767 literature.<sup>29</sup> The biggest obstacle for decellularization is to get rid of cellular components  
24  
25 768 (including RNA and DNA); hence, minimizing the immune response, while retaining the  
26  
27 769 inherent bioactive molecules. DAPI and H&E staining of NS and ADM reveal the absence of  
28  
29 770 cells in the ADM; further, DNA quantification supported successful decellularization of ADM.  
30  
31 771 The DNA content of ADM ( $30.14 \pm 12.34$  ng/mg dry wt.) is less than the minimal criterion  
32  
33 772 (50 ng/mg dry wt.) required for complete decellularization.<sup>65</sup> To emulate the intricacy of the  
34  
35 773 NS, ADM must retain multifarious structural and functional proteins, GAGs, glycoproteins and  
36  
37 774 bioactive cues (growth factors and cytokines), which are unique features of NS. Both NS and  
38  
39 775 ADM were observed to have non-significant difference in collagen and GAG contents and  
40  
41 776 these results were consistent with the literature.<sup>36</sup> Further, SDS-PAGE of NS and ADM  
42  
43 777 revealed the presence of several similar bands of similar intensities revealing the complexity  
44  
45 778 of ECM which was maintained during decellularization process. Moreover, ELISA assay  
46  
47 779 showed the presence of TGF- $\beta$ , VEGF and BMP-2 in both NS and ADM. TGF- $\beta$  plays an  
48  
49 780 essential role in cell proliferation and differentiation, immune response, angiogenesis, and  
50  
51 781 tissue repair. It also assists in the production of new matrix in graft and promotes graft  
52  
53 782 acceptance.<sup>66,67</sup> BMP2 serves as a chemotactic guide to graft for host cells, induces  
54  
55 783 adipogenesis in soft tissue spaces and promotes stem cell differentiation.<sup>68</sup> VEGF is reported  
56  
57 784 to induce cell migration and neovascularization in the newly formed tissue.<sup>69</sup>

53 785 Ideal skin substitute should mimic the native ECM proteins structurally that provides  
54  
55 786 mechanical support and also biologically active that helps in regulating cellular activities. In  
56  
57 787 native tissue ECM, collagen fibrils exist in a 3D network structure composed of multi-layered  
58  
59 788 nano fibrils (10–500 nm).<sup>70</sup> Our fabricated hybrid hydrogels are 3D networks which are  
60  
789 fibrillar owing to phase separation induced by physiological pH and temperature, as

1  
2  
3 790 demonstrated by SEM (fibril size: 90-120 nm). Interestingly, DHF-I cross-linking did not affect  
4  
5 791 the self-assembly of fiber formation in the hydrogel although the fiber diameter reduced after  
6  
7 792 crosslinking, yet it was not significantly different from the uncrosslinked variant. Also, the  
8  
9 793 triple helix structure of collagen was intact in both CCol-Cl and CsADM-Cl, as demonstrated  
10  
11 794 by FTIR data. CsADM-Cl immunostaining revealed the presence Col I, fibronectin, Col III,  
12  
13 795 VEGF, IL-8, and MCP-1. IL-8 is reported to promote skin reepithelialization by increasing  
14  
15 796 keratinocyte migration and MCP-1 has been utilized in literature to promote dermal wound  
16  
17 797 healing by acting as a chemo attractant for the cells.<sup>71-73</sup> DHF-I crosslinking enhanced the  
18  
19 798 mechanical strength of the hydrogel, crosslinked hydrogels were approximately double in  
20  
21 799 strength when compared to uncrosslinked variant (as revealed by rheological study).

22 800 Wound healing may be hindered by the bacterial load present on the chronic wounds;  
23  
24 801 since, the high bacterial load present on the wound site delays the wound healing by  
25  
26 802 upregulating MMP production, which in turns adversely affects collagen deposition and  
27  
28 803 remodeling. To reduce the wound region's bacterial load, the antibacterial skin substitute is  
29  
30 804 required. Herein, we have taken low molecular weight CTS for the study, since it has been  
31  
32 805 reported for its antibacterial property. Further, DHF-I crosslinking synergizes with the  
33  
34 806 polymer's inherent property, and the hybrid is observed to have excellent antibacterial property  
35  
36 807 against *E. coli* and *S. aureus* taken for the study. Antimicrobial activity of iodine has been  
37  
38 808 reported not only against bacteria but also fungi, tubercle bacilli and viruses; additionally,  
39  
40 809 bacteria does not develop resistance against iodine unlike antibiotics. Iodine is vital component  
41  
42 810 of thyroid hormone; hence, biologically safe and can be excreted by the kidneys.<sup>11</sup> The  
43  
44 811 antibacterial property therefore can be attributed to release of iodine from the crosslinked  
45  
46 812 hybrid hydrogel. It has also been reported in literature that iodine has antibacterial property  
47  
48 813 owing to its irreversible reaction to tyrosine residues/sites of unsaturation in lipids, oxidation  
49  
50 814 of sulfhydryl group, and interference in H-bonding of certain amino acid/nucleic acid.<sup>74</sup> The  
51  
52 815 release of iodine may be due to instability of di-iodinated compound in room temperature/light  
53  
54 816 leading to tendency to revert to iodine and olefin. Iodine, being an acceptor, is able to form  
55  
56 817 complexes with donor compounds. The complex is reported to be weak when formed with  
57  
58 818 ethers, esters, benzene and ketones using polar solvents, while it forms strong complex with  
59  
60 819 amino group containing compounds like triethylamine/pyridine.<sup>75</sup> However, the exact  
61  
62 820 mechanism of the release of elemental iodine from hybrid is not established. Thus, antibacterial  
63  
64 821 CsADM-Cl containing peptides, GAGs, cytokines and growth factors can act as an apt matrix  
65  
66 822 for facilitating rapid wound closure, when compared to CCol-Cl.

1  
2  
3 823 Skin mainly consists of fibroblast and keratinocytes cells; while, stem cells and  
4  
5 824 melanocytes are present in small number. Fibroblast or keratinocyte or both have been utilized  
6  
7 825 for assessment of grafts potential as a skin substitute *in vitro*. Hence, both fibroblast and  
8  
9 826 keratinocytes were selected for *in vitro* biological evaluation of hydrogel. In the present study,  
10  
11 827 conditioning media of the hydrogels revealed the absence of any toxic remnant chemicals,  
12  
13 828 while promoted cell adhesion, migration and proliferation of cells (HFCs and HKCs). All these  
14  
15 829 cell fate processes are confirmed using a spectrum of assays, including MTT assay, scratch  
16  
17 830 assay and Rhodamine & DAPI staining. The hybrid hydrogel showed uniform viable  
18  
19 831 cellularization on blending the pre-gel solution and fibroblast cells, i.e. as demonstrated by  
20  
21 832 Live/Dead staining post 3 days of encapsulation. Further, no apoptotic cell could be observed  
22  
23 833 in any of the hydrogel posts 7 days seeding, revealing the excellent cytocompatibility of the  
24  
25 834 hydrogels. In addition, cells were observed to be actively proliferating on hydrogel-coated  
26  
27 835 coverslips, when stained with PCNA staining. Interestingly, statistically higher ( $p < 0.001$ )  
28  
29 836 PCNA positive cells were found on CsADM-Cl coated coverslips. This may be attributed to  
30  
31 837 bioactive molecules in CsADM-Cl.

32  
33 838 Angiogenesis is a vital aspect in wound healing cascade, which governs initial  
34  
35 839 granulation tissue formation and tissue remodeling.<sup>61,62</sup> Moreover, insufficient vasculature can  
36  
37 840 cause necrosis, ultimately leading to rejection of the graft. In this context, angiogenic potential  
38  
39 841 of CsADM-Cl was demonstrated by *ex vivo* CAM assay. CsADM-Cl hydrogel implant was  
40  
41 842 observed to attract significantly higher number of allantoic vessels, when compared to CCol-  
42  
43 843 Cl hydrogel implanted CAM. The angiogenic property may be assigned to growth factors  
44  
45 844 (TGF- $\beta$  and VEGF), preserved during decellularization and fabrication process. The good  
46  
47 845 injectability of the crosslinked hydrogel was established by injecting the pre-gel solution into  
48  
49 846 the rat subcutaneous tissue. The qualitative and quantitative outcome of *in vivo* experiments  
50  
51 847 clearly indicated that the new hybrid hydrogel is suitable as an injectable material for minimally  
52  
53 848 invasive surgery. Histological assessment of the hydrogels revealed *in vivo* degradation of the  
54  
55 849 hydrogel and also good attachment of remnant hydrogel to the host tissue was observed. The  
56  
57 850 degradation of the hydrogel would release many bioactive components, such as peptides, which  
58  
59 851 are useful for recruitment of cell and tissue remodeling, although many components are still  
60  
61 852 unknown. CsADM-Cl injected group showed more infiltration of cells, when compared to  
62  
63 853 CCol-Cl injected group. The cell infiltration into the scaffolds is especially useful for tissue  
64  
65 854 remodeling and regeneration. In addition, no immune cell or capsular protein layer  
66  
67 855 encapsulating hydrogel was observed in any of the group. Iodine is known for its toxicity, so  
68  
69 856 to ensure non-toxic degradation of hydrogel vital organs were harvested and histological

1  
2  
3 857 evaluation was performed. All the organs showed similar histological morphology to  
4  
5 858 control/untreated group and characteristic morphological features can be easily identified  
6  
7 859 revealing the non-toxic nature of the CCol-Cl and CsADM-Cl upon degradation.

8  
9 860 The biomedical potential of CCol-Cl and CsADM-Cl to treat chronic wounds was  
10  
11 861 assessed in thermal burn wounds created in a rat model. Extracellular matrix from the tissue of  
12  
13 862 origin is the best alternative for regeneration as it contains all the proteins, proteoglycans,  
14  
15 863 glycosaminoglycans, cytokines and growth factors required for normal functioning of the  
16  
17 864 tissue.<sup>70</sup> Also, the presence of iodine in the hydrogel protected the wound bed from bacterial  
18  
19 865 infection and free radical load, which otherwise can delay the healing progression therein.<sup>76,77</sup>  
20  
21 866 CsADM-Cl treated wounds were observed to be rapidly closing with enhanced  
22  
23 867 reepithelialisation when compared to control or CCol-Cl treated group. Moreover, CsADM-Cl  
24  
25 868 treated wounds showed the development of more organized / structured collagen deposition,  
26  
27 869 which is much closer to the distribution of collagen in native tissue. Further, collagen index of  
28  
29 870 CsADM-Cl treated wounds was close to the native skin as reported in literature. The presence  
30  
31 871 of proteins, GAGs, cytokines and growth factors (CK-8, MCP-1, TGF- $\beta$ , VEGF and others not  
32  
33 872 quantified) in CsADM-Cl along with nanoscale fibrillar topology provided ambient  
34  
35 873 biochemical and physiological cues for rapid tissue regeneration. Genes profiling post 21 days  
36  
37 874 for the healing tissue also supported our data. COL I was upregulated in all the group revealing  
38  
39 875 the progression of the healing process, i.e. conversion of COL III to COL I; with, expression  
40  
41 876 being strongest in CsADM-Cl. In addition, COL III, KRT 10 and KRT 14 were down-regulated  
42  
43 877 in CsADM-CL demonstrating more complete tissue regeneration when compared to  
44  
45 878 SHAM/CCol-Cl. Taken together, our study demonstrates that CsADM-Cl hydrogel promoted  
46  
47 879 rapid wound closure, enhanced neovascularization, and complete skin regeneration post 21  
48  
49 880 days of wounding with superior well defined DEJ, collagen index native to NS, and skin  
50  
51 881 appendages. Thus, CsADM-Cl hydrogel holds significant potential to serve as a unique graft  
52  
53 882 for superior treatment of dermal wounds in clinical applications.

## 50 883 **5. Conclusion**

51  
52 884 An injectable hybrid hydrogel CsADM-Cl derived from the rat dermal tissue was  
53  
54 885 developed through modified decellularization, pepsin digestion and crosslinker. The newly  
55  
56 886 fabricated CsADM-Cl hydrogel successfully retained cytokines and growth factors, which  
57  
58 887 have the potential to guide the tissue regeneration even in chronic conditions. The CsADM-Cl  
59  
60 888 hydrogel exhibited a fibrous morphology and also, gel strength can be tailored by altering

1  
2  
3 889 crosslinker's concentration. The CsADM-Cl exhibited excellent antibacterial activity against  
4 890 *E.coli* and *S.aureus* and good cytocompatibility with HFC and HKCs, *in vitro*. HFC's were  
5 891 easily encapsulated into the CsADM-Cl hydrogel and proliferated well inside. Importantly, the  
6 892 CsADM-Cl hydrogel allowed a rapid cell infiltration *in vitro* and *in vivo*. It possessed superior  
7 893 angiogenic potential and was observed to be nonimmunogenic without toxicity to major organs  
8 894 studied. Moreover, the CsADM-Cl hydrogel treated wounds were completely healed with well-  
9 895 defined dermal-epidermal junctions and more pronounced secondary appendages. Altogether,  
10 896 our study clearly demonstrates that the CsADM-Cl hydrogel with its nanofibrillar topography,  
11 897 physiochemical composition, antibacterial activity, and injectability can serve as an apt graft  
12 898 for rapid wound healing in chronic wounds.

## 21 899 **Associated Content**

23 900 **Data Availability.** Data will be made available on request.

26 901 **Supporting Information.** Histological studies, DNA quantification, SDS PAGE, sGAG assay,  
27 902 Collagen quantification, Primer sequences

30 903 **Acknowledgement.** Authors acknowledge fellowship received from Department of Science  
31 904 and Technology (DST, Govt. of India) for Kamakshi Bankoti and Ministry of Human Resource  
32 905 Development (MHRD, Govt. of India) for Sayanti Datta and Arun Prabhu Rameshbabu. Nantu  
33 906 Dogra is acknowledged for helping in laboratory experiments. Project  
34 907 (BT/PR7818/MED/32/279/2013) funding from the Department of Biotechnology is  
35 908 acknowledged.

## 41 909 **6. References**

- 44 910 (1) Loo, Y.; Wong, Yong-Chiat; Cai, E. Z.; Ang, Chuan-Han; Raju, A.; Lakshmanana, A.;  
45 911 Koh, A. G.; Zhou, H. J.; Lim, Thiam-Chye; Moochhala, S. M.; Hauser, C. A. E.  
46 912 Ultrashort Peptide Nanofibrous Hydrogels for the Acceleration of Healing of Burn  
47 913 Wounds. *Biomaterials* **2014**, *35*, 4805–4814.
- 48 914 (2) Selig, H. F.; Lumenta, D. B.; Giretzlehner, M.; Jeschke, M. G.; Upton, D.; Kamolz, L.  
49 915 P. The Properties of an “Ideal” Burn Wound Dressing – What Do We Need in Daily  
50 916 Clinical Practice? Results of A Worldwide Online Survey Among Burn Care  
51 917 Specialists. *Burns* **2012**, *38*, 960–966.

- 1  
2  
3 918 (3) Ravishanker, R.; Bath, R.; Roy, R. Amnion Bank-The Use of Long-Term Glycerol  
4 919 Preserved Amniotic Membranes in the Management of Superficial and Superficial  
5 920 Partial-Thickness Burns. *Burns* **2003**, *29*, 369–374.
- 6  
7  
8 921 (4) Gist, S.; Iris, T. M.; Falzgraf, S.; Cameron, S.; Beebe, M. Wound Care in the Geriatric  
9 922 Client. *Clin. Interv. Aging* **2009**, *4*, 269–287.
- 10  
11 923 (5) Okan, D.; Woo, K. E.; Ayello, A.; Sibbald, G. The Role of Moisture Balance in  
12 924 Wound Healing. *Adv. Skin Wound Care* **2007**, *20*, 39–53.
- 13  
14 925 (6) Hrynyk, M.; Martins-Green, M.; Barron, A. E.; Neufeld, R. J. Alginate-PEG Sponge  
15 926 Architecture and Role in The Design of Insulin Release Dressings. *Biomacromolecules*  
16 927 **2012**, *13*, 1478–1485.
- 17  
18 928 (7) Liu, Y.; Petreaca, M.; Martins-Green, M. Cell and Molecular Mechanisms of Insulin-  
19 929 Induced Angiogenesis. *J. Cell Mol. Med.* **2009**, *13*, 4492–4504.
- 20  
21 930 (8) Ito, T.; Fraser, I. P.; Yeo, Y.; Highley, C. B.; Bellas, E.; Kohane, D. S. Anti-  
22 931 Inflammatory Function of an In Situ Cross-Linkable Conjugate Hydrogel of Hyaluronic  
23 932 Acid and Dexamethasone. *Biomaterials* **2007**, *28*, 1778–86.
- 24  
25 933 (9) Salick, D. A.; Kretsinger, J. K.; Pochan, D. J.; Schneider, J. P. Inherent Antibacterial  
26 934 Activity of a Peptide-Based Beta-Hairpin Hydrogel. *J. Am. Chem. Soc.* **2007**, *129*,  
27 935 14793–14799.
- 28  
29 936 (10) McDonnell, G.; Russell, A. D. Antiseptics and Disinfectants: Activity, Action, and  
30 937 Resistance. *Clin. Microbiol. Rev.* **1999**, *12*, 147–179.
- 31  
32 938 (11) Shirai, T.; Shimizu, T.; Ohtani, K.; Zen, Y.; Takaya, M.; Tsuchiya, H. Antibacterial  
33 939 Iodine-Supported Titanium Implants. *Acta Biomater.* **2011**, *7*, 1928–1933.
- 34  
35 940 (12) Durani, P.; Leaper, D. Povidone–Iodine: Use in Hand Disinfection, Skin Preparation  
36 941 and Antiseptic Irrigation. *Int. Wound J.* **2008**, *5*, 376–387.
- 37  
38 942 (13) Ong, S. Y.; Wu, J. S.; Moochhala, M.; Tan, M. H.; Lu, J. Development of a Chitosan-  
39 943 Based Wound Dressing with Improved Hemostatic and Antibacterial Properties.  
40 944 *Biomaterials* **2008**, *29*, 4323–4332.
- 41  
42 945 (14) Kim, I.; Seo, S.; Moon, H.; Yoo, M.; Park, I.; Kim, B.; Cho, C. Chitosan and its  
43 946 Derivatives for Tissue Engineering Applications. *Biotechnol. Adv.* **2008**, *26*, 1–21.
- 44  
45 947 (15) Sana, F. A.; Yurtsever, M. C.; Bayrak, G. K.; Tuncay, E. O.; Kiremitci, A. S.;  
46 948 Gumusderelioglu, M. Spreading, Proliferation and Differentiation of Human Dental  
47 949 Pulp Stem Cells on Chitosan Scaffolds Immobilized with RGD or Fibronectin.  
48 950 *Cytotechnology* **2017**, *69*, 617–630.
- 51  
52  
53  
54  
55  
56  
57  
58  
59  
60



- 1  
2  
3 951 (16) Liu H.; Fan, H.; Cui, Y.; Chen, Y.; Yao, K.; Goh, J.C.H. Effects of The Controlled-  
4 952 Released Basic Fibroblast Growth Factor from Chitosan–Gelatin Microspheres on  
5 953 Human Fibroblasts Cultured on A Chitosan–Gelatin Scaffold. *Biomacromolecules*  
6 954 **2007**, *8*, 1446–1455.
- 7  
8  
9  
10 955 (17) Ikemoto, S.; Mochizuki, M.; Yamada, M.; Takeda, A.; Uchinuma, E.; Yamashina, S.;  
11 956 Nomizu, M.; Kadoya, Y. Laminin Peptide-Conjugated Chitosan Membrane:  
12 957 Application for Keratinocyte Delivery in Wounded Skin. *J. Biomed. Mater. Res. A* **2006**,  
13 958 *79*, 716–722.
- 14  
15  
16  
17 959 (18) Hozumi, K.; Yamagata, N.; Otagiria, D.; Fujimori, C.; Kikkawa, Y.; Kadoya Y.;  
18 960 Nomizu, M. Mixed Peptide–Chitosan Membranes to Mimic the Biological Activities of  
19 961 a Multifunctional Laminin A1 Chain LG4 Module. *Biomaterials* **2009**, *30*, 1596–1603.
- 20  
21  
22 962 (19) Ma, L.; Gao, C.; Mao, Z.; Zhou, J.; Shen, J.; Hu, X.; Han, C. Collagen/Chitosan Porous  
23 963 Scaffolds with Improved Biostability For Skin Tissue Engineering. *Biomaterials* **2003**,  
24 964 *24*, 4833–4841.
- 25  
26  
27 965 (20) Ueno, H.; Mori, T.; Fujinaga, T. Topical Formulations and Wound Healing  
28 966 Applications of Chitosan. *Adv. Drug Delivery Rev.* **2001**, *52*, 105–115.
- 29  
30  
31 967 (21) Lecht, S.; Stabler, C. T.; Rylander, A. L.; Chiaverelli, R.; Schulman, E. S.;  
32 968 Marcinkiewicz, C.; Lelkes, P. I. Enhanced Reseeding of Decellularized Rodent Lungs  
33 969 with Mouse Embryonic Stem Cells. *Biomaterials* **2014**, *35*, 3252–3262.
- 34  
35  
36 970 (22) Watt, F. M.; Huck, W. T. S. Role of The Extracellular Matrix in Regulating Stem Cell  
37 971 Fate. *Nat. Rev. Mol. Cell Biol.* **2013**, *14*, 467– 473.
- 38  
39  
40 972 (23) Clause, K. C.; Barker, T. H. Extracellular Matrix Signaling in Morphogenesis and  
41 973 Repair. *Curr. Opin. Biotechnol.* **2013**, *24*, 830–833.
- 42  
43 974 (24) Reing, J. E.; Zhang, L.; Myers-Irvin, J.; Cordero, K. E.; Freytes, D. O.; Heber-Katz,  
44 975 E.; Bedelbaeva, K.; McIntosh, D.; Dewilde, A.; Braunhut, S. J.; Badylak, S. F.  
45 976 Degradation Products of Extracellular Matrix Affect Cell Migration and Proliferation.  
46 977 *Tissue Eng., Part A* **2009**, *15*, 605–614.
- 47  
48  
49 978 (25) Brennan, E. P.; Tang, Xiao-Han.; Stewart-Akers, A. M.; Gudas, L. J.; Badylak, S. F.  
50 979 Chemoattractant Activity of Degradation Products of Fetal and Adult Skin Extracellular  
51 980 Matrix for Keratinocyte Progenitor Cells. *J. Tissue Eng. Regener. Med.* **2008**, *2*, 491–  
52 981 498.
- 53  
54  
55 982 (26) Yang, Q.; Peng, J.; Guo, Q.; Huang, J.; Zhang, L.; Yao, J.; Yang, F.; Wang, S.; Xu,  
56 983 W.; Wang, A.; Lu, S. A Cartilage ECM-Derived 3-D Porous Acellular Matrix Scaffold  
57  
58  
59  
60

- 1  
2  
3 984 For In Vivo Cartilage Tissue Engineering With PKH26-Labeled Chondrogenic Bone  
4 Marrow-Derived Mesenchymal Stem Cells. *Biomaterials* **2008**, *29*, 2378–2387.
- 5 985  
6 986 (27) Gilbert, T. W.; Sellaro, T. L.; Badylak, S. F. Decellularization of tissues and organs,  
7 *Biomaterials* **2006**, *27*, 3675–3683.  
8 987  
9 988 (28) Lee, J. S.; Shin, J.; Park, H.; Kim, Y.; Kim, B.; Oh, J.; Cho, S. Liver Extracellular  
10 Matrix Providing Dual Functions of Two-Dimensional Substrate Coating and Three-  
11 Dimensional Injectable Hydrogel Platform for Liver Tissue Engineering.  
12 *Biomacromolecules* **2014**, *15*, 206–218.  
13 990  
14 991 (29) Wolf, M. T.; Daly, K. A.; Brennan-Pierce, E. P.; Johnson, S. A.; Carruthers, C. A.;  
15 D'Amore, A.; Nagarkar, S. P.; Velankar, S. S.; Badylak, S. F.; A Hydrogel Derived  
16 from Decellularized Dermal Extracellular Matrix, *Biomaterials* **2012**, *33*, 7028–38.  
17 992  
18 993 (30) Young, B. M.; Shankar, K.; Allen, B. P.; Pouliot, R. A.; Schneck, M. B.; Mikhael, N.  
19 S., Heise, R. L. Electrospun decellularized lung matrix scaffold for airway smooth  
20 muscle culture, *ACS Biomater. Sci. Eng.* **2017**, *3*, 3480–3492.  
21 994  
22 995 (31) Efrain, Y.; Sarig, H.; Anavya, N. C.; Sarig, U.; Berardinis, Elio de.; Chaw, S.;  
23 Krishnamoorthi, M.; Kalifa, J.; Bogireddi, H.; Duc, Thang Vu.; Kofidis, T.L.; Baruch,  
24 B.; Venkatraman, S. S.; Machluf, M. Biohybrid Cardiac ECM-Based Hydrogels  
25 Improve Long Term Cardiac Function Post Myocardial Infarction, *Acta Biomater.*  
26 **2017**, *50*, 220–233.  
27 1000  
28 1001 (32) Gupta, V.; Lyne, D. V.; Laflin, A. D.; Zabel, T. A.; Barragan, M.; Bunch, J. T.;  
29 Pacicca, D. M.; Detamore, M. S. Microsphere-Based Osteochondral Scaffolds Carrying  
30 Opposing Gradients of Decellularized Cartilage and Demineralized Bone Matrix. *ACS*  
31 *Biomater. Sci. Eng.* **2017**, *3*, 1955–1963.  
32 1002  
33 1003 (33) Rameshbabu, A. P.; Bankoti, K.; Datta, S.; Subramani, E.; Apoorva, A.; Ghosh, P.;  
34 Maity, P.P.; Manchikanti, P.; Chaudhury, K.; Dhara, S. Silk Sponges Ornamented With  
35 A Placenta-Derived Extracellular Matrix Augment Full-Thickness Cutaneous Wound  
36 Healing By Stimulating Neovascularization And Cellular Migration. *ACS Appl. Mater.*  
37 *Interfaces* **2018**, *10*, 16977–16991.  
38 1004  
39 1005 (34) Jichuan, Q.; Jianhua, L.; Guancong, W.; Lin, Z.; Na, R.; Hong, L.; Wei, T.; Huaidong,  
40 J.; Yingjun, W. In Vitro Investigation on The Biodegradability And Biocompatibility  
41 Of Genipin Cross-Linked Porcine Acellular Dermal Matrix With Intrinsic  
42 Fluorescence, *ACS Appl. Mater. Interfaces* **2013**, *5*, 344–350.  
43 1007  
44 1008 (35) Kumar, N.; Gangwar, A. K.; Sharma, A. K.; Negi, M.; Shrivastava, S.; Mathew, D.  
45 D.; Sonal, V. R.; Maiti, S. K.; Devi, Kh. S.; V.; Ramteke, P. W.; Kaarthick, D. T.;  
46 1009  
47 1010  
48 1011  
49 1012  
50 1013  
51 1014  
52 1015  
53 1016  
54 1017

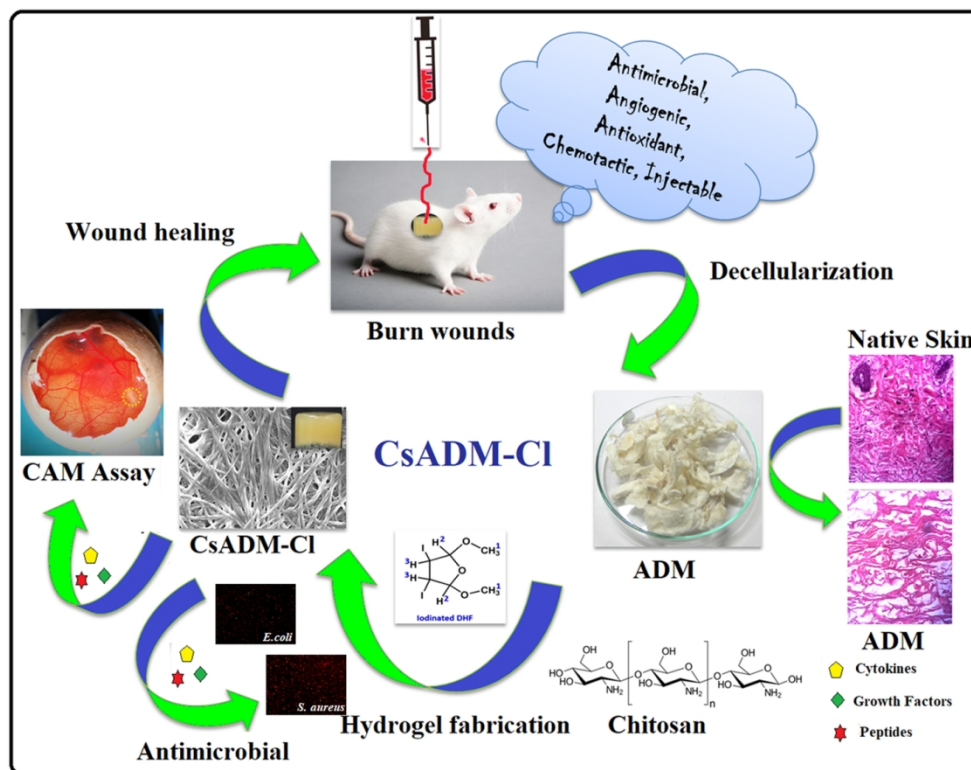
- 1  
2  
3 1018 Kurade, N. P. Extraction Techniques for The Decellularization of Rat Dermal  
4  
5 1019 Constructs. *Trends Biomater. Artif. Organs* **2013**, *27*, 102–107.  
6  
7 1020 (36) Reing, J. E.; Brown, B. N.; Daly, K. A.; Freund, J. M.; Gilbert, T. W.; Hsiong, S. X.;  
8  
9 1021 Huber, A.; Kullas, K. E.; Tottey, S.; Wolf, M. T.; Badylak, S. F. The Effects of  
10 1022 Processing Methods Upon Mechanical and Biologic Properties of Porcine Dermal  
11 1023 Extracellular Matrix Scaffolds. *Biomaterials* **2010**, *31*, 8626–8633.  
12  
13 1024 (37) Rajan, N.; Habermehl, J.; Coté, M. F.; Doillon, C. J.; Mantovani, D. Preparation of  
14 1025 Ready-To-Use, Storable and Reconstituted Type I Collagen from Rat Tail Tendon for  
15 1026 Tissue Engineering Applications. *Nat. Protoc.* **2006**, *1*, 2753–2758.  
16  
17 1027 (38) Ghosh, P.; Das, M.; Rameshbabu, A. P.; Das, D.; Datta, S.; Pal, S.; Panda, A. B.;  
18 1028 Dhara, S. Chitosan Derivatives Cross-Linked with Iodinated 2,5-Dimethoxy-2,5-  
19 1029 Dihydrofuran for Non-Invasive Imaging. *ACS Appl. Mater. Interfaces* **2014**, *6*, 17926–  
20 1030 17936.  
21  
22 1031 (39) Zhao, X.; Wu, H.; Guo, B.; Dong, R.; Qiu, Y.; Ma, P. X. Antibacterial Anti-Oxidant  
23 1032 Electroactive Injectable Hydrogel as Self- Healing Wound Dressing with Hemostasis  
24 1033 and Adhesiveness For Cutaneous Wound Healing, *Biomaterials* **2017**, *122*, 34–47.  
25  
26 1034 (40) Punnakitikashem P.; Truong, D.; Menon, J. U.; Nguyen, K. T.; Hong, Y. Electrospun  
27 1035 Biodegradable Elastic Polyurethane Scaffolds with Dipyridamole Release for Small  
28 1036 Diameter Vascular Grafts. *Acta Biomater.* **2014**, *10*, 4618–4628.  
29  
30 1037 (41) Li, P.; Poon, Y. F.; Li, W.; Zhu, H. Y.; Yeap, S. H.; Cao, Y.; Qi, X.; Zhou, C.; Lamrani,  
31 1038 M., Beuerman, R. W.; Kang, E. T.; Mu, Y., Li, C.M.; Chang, M.W.; Leong, S. S. J.;  
32 1039 Chan-Park, M. B.; A Polycationic Antimicrobial and Biocompatible Hydrogel with  
33 1040 Microbe Membrane Suctioning. Ability. *Nat. Mater.* **2010**, *10*, 149–156.  
34  
35 1041 (42) Aasen, T.; Belmonte, J.C.I. Isolation and Cultivation of Human Keratinocytes from  
36 1042 Skin or Plucked Hair for The Generation of Induced Pluripotent Stem Cells. *Nat.*  
37 1043 *Protoc.* **2010**, *5*, 371–382.  
38  
39 1044 (43) Sun, G.; Zhang, X.; Shen, Y.; Sebastain, R.; Dickinson, L. E.; Fox-Talbot, K.;  
40 1045 Reinblatt, M.; Steenbergen, C.; Harmon, J. W.; Gerecht, S. Dextran Hydrogel Scaffolds  
41 1046 Enhance Angiogenic Responses and Promote Complete Skin Regeneration During  
42 1047 Burn Wound Healing, *Proc. Natl. Acad. Sci. U. S. A.* **2011**, *108*, 20976–20981.  
43  
44 1048 (44) Terzi, E.; Storelli, S.; Bettini, T.; Sibillano, D.; Altamura, L.; Salvatore, M.;  
45 1049 Madaghiele, A.; Romano, D.; Siliqi, M.; Ladisa, L.; De Caro, A.; Quattrini, L.; Valli,  
46 1050 A.; Sannino, C. G. Effects of Processing on Structural, Mechanical and Biological  
47  
48  
49  
50  
51  
52  
53  
54  
55  
56  
57  
58  
59  
60

- 1  
2  
3 1051 Properties of Collagen-Based Substrates for Regenerative Medicine. *Sci. Rep.* **2018**, *8*,  
4 1052 1429.  
5  
6 1053 (45) Fernandes, L. L.; Resende, C. X.; Tavares, D. S.; Soares, G. A.; Castro, L. O.;  
7 1054 Granjeiro, J. M. Cytocompatibility of Chitosan and Collagen-Chitosan Scaffolds for  
8 1055 Tissue Engineering. *Polimeros* **2011**, *21*, 1–6.  
9  
10 1056 (46) Huang, Y.; Wang, Y.; Chen, L.; Zhang, L. Facile Construction of Mechanically  
11 1057 Tough Collagen Fibers Reinforced by Chitin Nanofibers as Cell Alignment Templates.  
12 1058 *J. Mater. Chem. B* **2018**, *6*, 918–929.  
13  
14 1059 (47) Sen, C. K.; Khanna, S.; Gordillo, G.; Bagchi, D.; Bagchi, M.; Roy, S. Oxygen,  
15 1060 Oxidants, and Antioxidants in Wound Healing, *Ann. N.Y. Acad. Sci.* **2002**, *957*, 239–  
16 1061 249.  
17  
18 1062 (48) Aceves, C.; Anguiano, B.; Delgado, G. The Extrathyronine Actions of Iodine as  
19 1063 Antioxidant, Apoptotic, and Differentiation Factor in Various Tissues, *Thyroid* **2013**,  
20 1064 *23*, 938–946.  
21  
22 1065 (49) Balaji, A.; Jaganathan, S. K.; Ismail, A. F.; Rajasekar, R. Fabrication and  
23 1066 Hemocompatibility Assessment of Novel Polyurethane-Based Bio-Nanofibrous  
24 1067 Dressing Loaded with Honey and *Carica Papaya* Extract for The Management of Burn  
25 1068 Injuries. *Int. J. Nanomed.* **2016**, *11*, 4339–4355.  
26  
27 1069 (50) Hemocompatibility results Document ASTM. Standard Practice for Assessment of  
28 1070 Hemolytic Properties of Materials Designation: F 756-00. *Annu. Book ASTM Stand.*  
29 1071 **2005**, 309–313.  
30  
31 1072 (51) Church, D.; Elsayed, S.; Reid, O.; Winston, B.; Lindsay, R. Burn Wound Infections.  
32 1073 *Clin. Microbiol Rev.* **2006**, *19*, 403–434.  
33  
34 1074 (52) Zubko, E. I.; Zubko, M. K. Co-Operative Inhibitory Effects of Hydrogen Peroxide  
35 1075 and Iodine Against Bacterial and Yeast Species. *B. M. C. Res. Notes* **2013**, *6*, 272–279.  
36  
37 1076 (53) Punyani, S.; Narayanan, P.; Vasudevan, P.; Singh, H. Sustained Release of Iodine  
38 1077 from a Polymeric Hydrogel Device for Water Disinfection. *J. Appl. Polym. Sci.* **2007**,  
39 1078 *103*, 3334–3340.  
40  
41 1079 (54) Raghov, R. The Role of Extracellular Matrix in Post Inflammatory Wound Healing  
42 1080 and Fibrosis. *FASEB J.* **1994**, *8*, 823–831.  
43  
44 1081 (55) Lawrence, W. T.; Diegelmann, R. F. Growth Factors in Wound Healing. *Clin.*  
45 1082 *Dermatol.* **1994**, *12*, 157–169.  
46  
47  
48  
49  
50  
51  
52  
53  
54  
55  
56  
57  
58  
59  
60

- 1  
2  
3 1083 (56) Greenwel, P.; Inagaki, Y.; Hu, W.; Walsh, M.; Ramirez, F.; Sp1 is Required for the  
4 1084 Early Response of A2 (I) Collagen to Transforming Growth Factor- $\beta$ 1. *J. Biol. Chem.*  
5 1085 **1997**, *272*, 19738–19745.  
6  
7  
8 1086 (57) Li, Z.; Zhou, F.; Li, Z.; Lin, S.; Chen, L.; Liu, L.; Chen, Y. Hydrogel Cross-Linked  
9 1087 with Dynamic Covalent Bonding and Micellization for Promoting Burn Wound  
10 1088 Healing. *ACS Appl. Mater. Interfaces* **2018**, *10*, 25194–25202.  
11  
12  
13 1089 (58) Metcalfe, A. D.; Ferguson, M. W. J. Tissue Engineering of Replacement Skin: The  
14 1090 Crossroads of Biomaterials, Wound Healing, Embryonic Development, Stem Cells and  
15 1091 Regeneration. *J. R. Soc., Interface* **2007**, *4*, 413–437.  
16  
17  
18 1092 (59) Rameshbabu, A. P.; Bankoti, K.; Datta, S.; Subramani, E.; A. Apoorva.; Ghosh. P.;  
19 1093 Maity, P. P.; Manchikanti, P.; Chaudhury, K.; Dhara, S. Silk Sponges Ornamented with  
20 1094 a Placenta-Derived Extracellular Matrix Augment Full-Thickness Cutaneous Wound  
21 1095 Healing by Stimulating Neovascularization and Cellular Migration. *ACS Appl. Mater.*  
22 1096 *Interfaces* **2018**, *10*, 16977–16991.  
23  
24  
25 1097 (60) Choi, J. U.; Lee, S. W.; Pageni, R.; Byun, Y.; Yoon, I.; Park, J. W. Preparation and  
26 1098 In Vivo Evaluation of Cationic Elastic Liposomes Comprising Highly Skin-Permeable  
27 1099 Growth Factors Combined with Hyaluronic Acid for Enhanced Diabetic Wound-  
28 1100 Healing Therapy. *Acta Biomater.* **2017**, *57*, 197–215.  
29  
30  
31 1101 (61) Madeddu P. Therapeutic Angiogenesis and Vasculogenesis for Tissue Regeneration,  
32 1102 *Exp. Physiol.* **2005**, *90*, 315–326.  
33  
34  
35 1103 (62) Nomi, M.; Atala, A.; Coppi, P. D.; Soker, S. Principals of Neovascularization for  
36 1104 Tissue Engineering. *Mol. Aspects Med.* **2002**, *23*, 463–483.  
37  
38  
39 1105 (63) Tan, Q.; Chen, B.; Yan, X.; Lin, Y.; Xiao, Z.; Hou, X.; Dai, J. Promotion of Diabetic  
40 1106 Wound Healing by Collagen Scaffold with Collagen Binding Vascular Endothelial  
41 1107 Growth Factor in A Diabetic Rat Model. *J. Tissue Eng. Regener. Med.* **2014**, *8*, 195–  
42 1108 201.  
43  
44  
45 1109 (64) Sun, G., Zhang, X.; Shena, Y.; Sebastian, R.; Dickinson, L. E.; Fox-Talbot, K.;  
46 1110 Reinblatt, M.; Steenbergen, C.; Harmon, Gerecht, J. W. S. Dextran Hydrogel Scaffolds  
47 1111 Enhance Angiogenic Responses and Promote Complete Skin Regeneration During  
48 1112 Burn Wound Healing. *Proc. Natl. Acad. Sci. U. S. A.* **2011**, *108*, 20976–20981.  
49  
50  
51 1113 (65) Crapo, P. M.; Gilbert, T. W.; Badylak, S. F. An Overview of Tissue and Whole Organ  
52 1114 Decellularization Processes. *Biomaterials* **2011**, *32*, 3233–3243.  
53  
54  
55 1115 (66) Penn, J. W.; Grobbelaar, A. O.; Rolfe, K. J. The Role of the TGF-B Family in Wound  
56 1116 Healing, Burns and Scarring: A Review. *Int. J. Burns Trauma* **2012**, *2*, 18–28.

- 1  
2  
3 1117 (67) Pakyari, M. Farrokhi, A.; Maharlooei, M. K.; Ghahary, A. Critical Role of  
4 1118 Transforming Growth Factor Beta in Different Phases of Wound Healing. *Adv. Wound*  
5 1119 *Care (New Rochelle)* **2013**, *2*, 215–224.  
6  
7  
8 1120 (68) Sottile, V.; Seuwen, K.; Bone Morphogenetic Protein-2 Stimulates Adipogenic  
9 1121 Differentiation of Mesenchymal Precursor Cells in Synergy with BRL 49653  
10 1122 (Rosiglitazone), *FEBS Lett.* **2000**, *475*, 201–204.  
11  
12 1123 (69) Johnson, K. E.; Wilgus, T. A. Vascular Endothelial Growth Factor and Angiogenesis  
13 1124 in the Regulation of Cutaneous Wound Repair. *Adv. Wound Care (New Rochelle)* **2014**,  
14 1125 *3*, 647–661.  
15  
16  
17 1126 (70) Mouw, J. K.; Ou, G.; Weaver, V. M. Extracellular Matrix Assembly: A Multiscale  
18 1127 Deconstruction. *Nat. Rev. Mol. Cell Biol.* **2014**, *15*, 771–785.  
19  
20 1128 (71) Engelhardt, E.; Toksoy, A.; Goebeler, M.; Debus, S.; Brocker, E. B.; Gillitzer, R.  
21 1129 Chemokines IL-8, Groalpha, MCP-1, IP-10, And Mig are Sequentially and  
22 1130 Differentially Expressed During Phase-Specific Infiltration of Leukocyte Subsets in  
23 1131 Human Wound Healing. *Am. J. Pathol.* **1998**, *153*, 1849–60.  
24  
25 1132 (72) Rennekampff, H.O.; Hansbrough, J. F.; Kiessig, V.; Dore, C.; Sticherling, M.;  
26 1133 Schroder, J. M. Bioactive Interleukin-8 Is Expressed in Wounds and Enhances Wound  
27 1134 Healing. *J. Surg. Res.* **2000**, *93*, 41–54.  
28  
29 1135 (73) Wood, S.; Jayaraman, V.; Huelsmann, E. J.; Bonish, B.; Burgad, D.;  
30 1136 Sivaramakrishnan, G.; Qin, S.; DiPietro, L. A.; Zloza, A.; Zhang, C.; Shafikhani, S. H.  
31 1137 Pro-Inflammatory Chemokine Ccl2 (Mcp-1) Promotes Healing in Diabetic Wounds by  
32 1138 Restoring the Macrophage Response. *PLoS One* **2014**, *9*, e91574.  
33  
34 1139 (74) Some, S.; Sohn, J. S.; Kim, J.; Su-Hyun Lee, S. C.; Lee, J.; Lee, I.; Shackery, S. K.;  
35 1140 Kim, S. H.; Kim, N.; Choi, I.; Jung, H.; Kang, S.; Jun, S. C. Graphene-Iodine  
36 1141 Nanocomposites: Highly Potent Bacterial Inhibitors that are Bio-Compatible with  
37 1142 Human Cells, *Sci. Rep.* **2016**, *6*, 2015.  
38  
39 1143 (75) Lacroix-Desmazes, P.; Severac, R.; Boutevin, B. Reverse Iodine Transfer  
40 1144 Polymerization of Methyl Acrylate and N-Butyl Acrylate. *Macromolecules* **2005**, *38*,  
41 1145 6299–6309.  
42  
43 1146 (76) Zhao, D.; Lim, C. P.; Miyanaga, K.; Tanji, Y. Iodine from Bacterial Iodide Oxidization  
44 1147 by *Roseovarius* Spp. Inhibits the Growth of other Bacteria, *Appl. Microbiol. Biotechnol.*  
45 1148 **2012**, *97*, 2173–2182.  
46  
47  
48  
49  
50  
51  
52  
53  
54  
55  
56  
57  
58  
59  
60

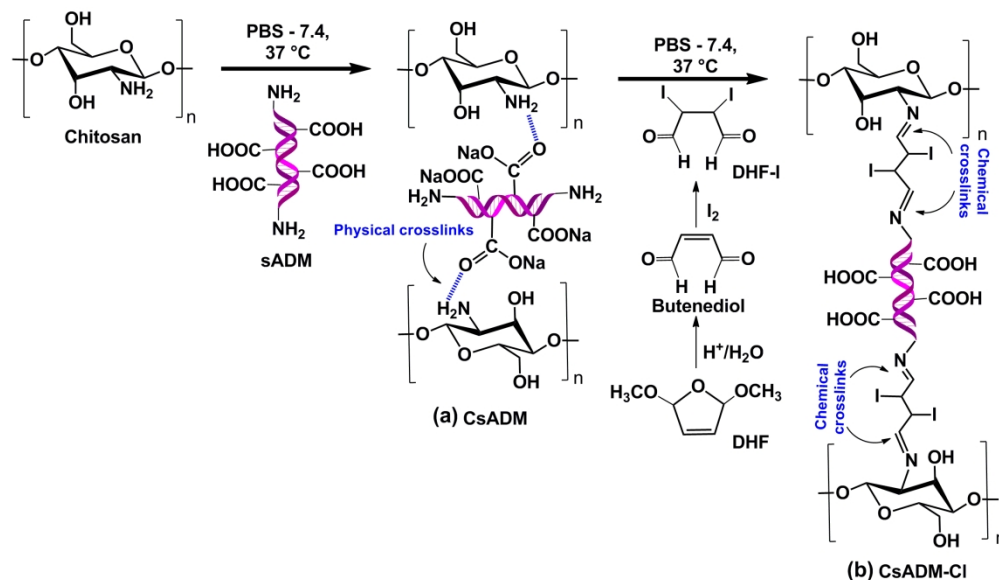
- 1  
2  
3 1149 (77) Beukelman, C. J.; van den Berg, A. J.; Hoekstra, M. J.; Uhl, R.; Reimer, K.; Mueller,  
4  
5 1150 S. Anti-Inflammatory Properties of a Liposomal Hydrogel with Povidone-Iodine  
6  
7 1151 (Repithel) for Wound Healing In Vitro. *Burns* **2008**, *34*, 845–855.  
8  
9 1152  
10  
11  
12  
13  
14  
15  
16  
17  
18  
19  
20  
21  
22  
23  
24  
25  
26  
27  
28  
29  
30  
31  
32  
33  
34  
35  
36  
37  
38  
39  
40  
41  
42  
43  
44  
45  
46  
47  
48  
49  
50  
51  
52  
53  
54  
55  
56  
57  
58  
59  
60



Graphical Abstract

127x99mm (300 x 300 DPI)





Schematics 1. Synthesis strategy of crosslinked hybrid hydrogel. Schematic representation of physical crosslinking between CTS and ADM at specific conditions to form hydrogel CsADM (a); further, CsADM was crosslinked using DHF-I to form CsADM-CI (b).

233x135mm (300 x 300 DPI)

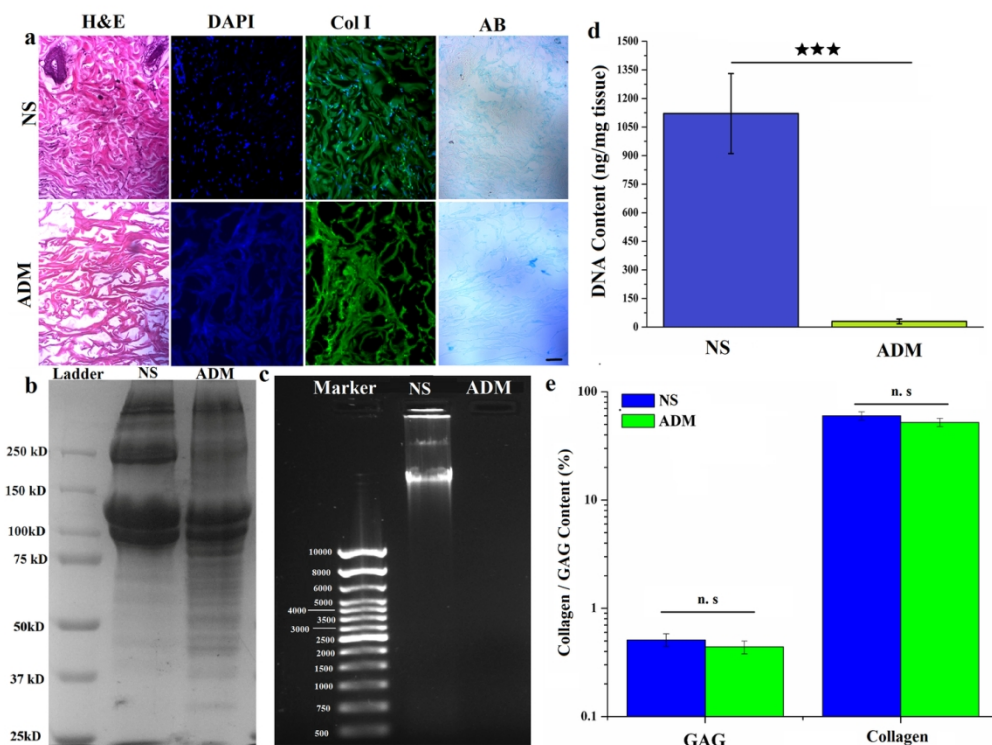


Fig. 1. Decellularized skin was used as acellular dermal matrix in developing crosslinked hydrogel. Histological and immunohistochemical analysis of NS and ADM (a), Total protein extracted from NS and ADM separated by SDS-PAGE (b), DNA isolation and quantification from NS and ADM (c, d), and quantification of GAGs and Collagen from NS and ADM (e). Scale bar represents 50  $\mu$ m, Y-error bars symbolize standard deviation, and \*\*\* signifies  $p < 0.001$ .

127x95mm (300 x 300 DPI)

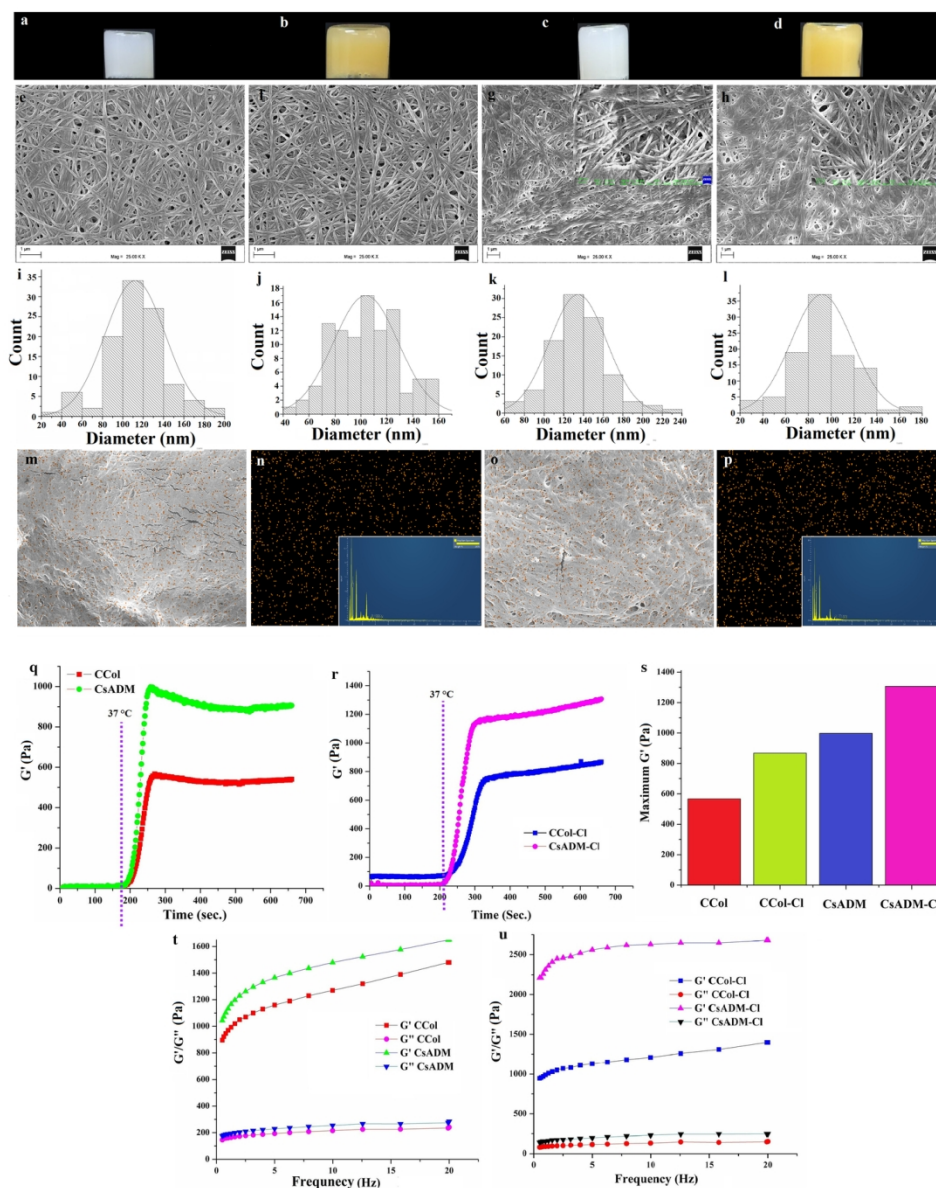


Fig. 2. Crosslinking enhances viscoelastic properties, while retaining nanofibrillar hydrogel architecture. Optical images, surface topology, and fiber network analysis of CCol (a, e, i), CCol-Cl (b, f, j), CsADM (c, g, k), and CsADM-Cl (d, h, l), inset (g & i) shows magnified images; EDX mapping of iodine on fibrillar network of CCol-Cl (m, n) and CsADM-Cl (o, p). Gelation kinetics of hydrogel (q) without crosslinker (CCol & CsADM) and (r) with crosslinker (CCol-Cl & CsADM-Cl); (s) maximum elastic modulus ( $G'$ ); frequency sweep analysis post gelation for (t) uncrosslinked (CCol & CsADM) and (u) crosslinked (CCol-Cl & CsADM-Cl) samples.

131x161mm (300 x 300 DPI)

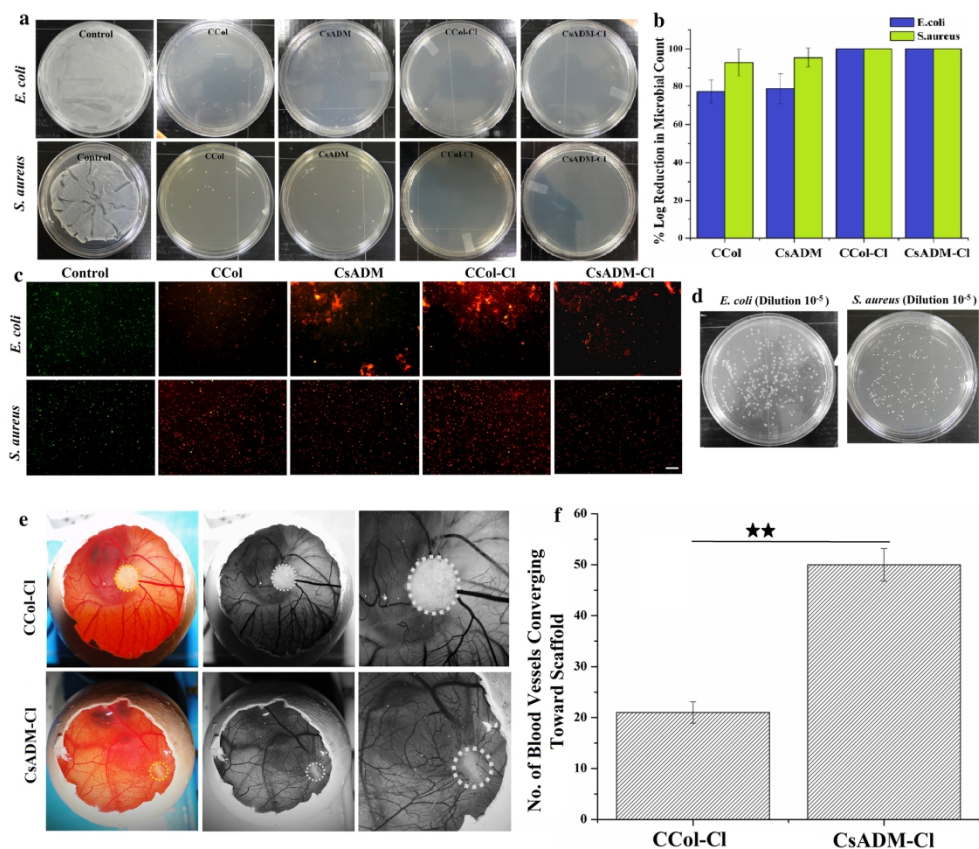


Fig. 3. Antimicrobial and angiogenic potential, both are important in wound healing applications. Microbes (*E. coli* and *S. aureus*) colony grown on agar plate after contact with control and hydrogel (a); log reduction in microbial count (b); Live/Dead staining post 2 h of incubation with hydrogel (c); and culture plates of control treated *E. coli* and *S. aureus* ( $10^{-5}$  dilution) (d). CAM assay macroscopic view (e) and quantification of vessels (f) growing towards scaffolds. Y-error bars represent standard deviation, \*\* signifies  $p < 0.01$ , Scale bar represent 50  $\mu\text{m}$ .

169x143mm (300 x 300 DPI)



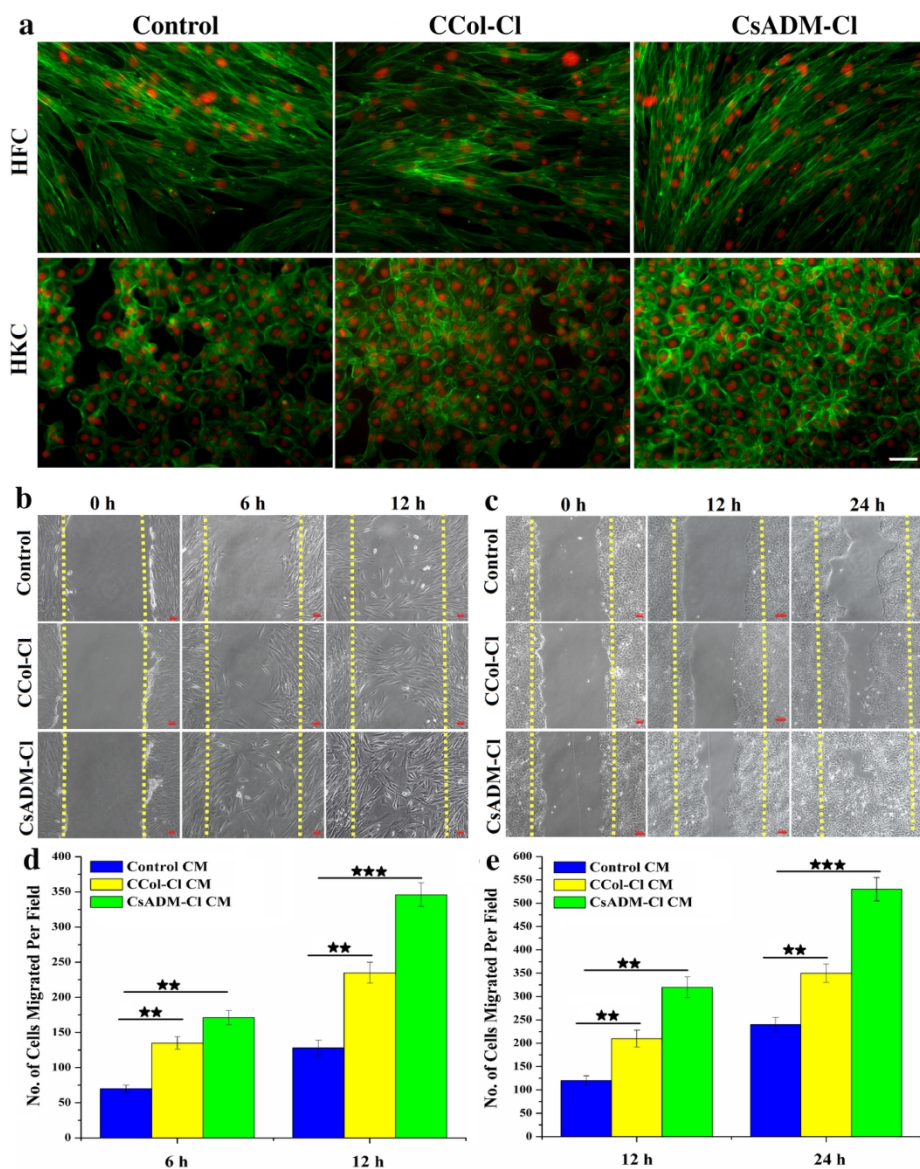


Fig. 4. Crosslinked hybrid hydrogels exhibit better cytocompatibility and cell migration behavior of skin tissue cells. Rhodamine phalloidin–DAPI images of HFCs and HKCs cultivated in CCol-CI and CsADM-CI-conditioned medium (a). Scratch assay images of (b) HFCs and (c) HKCs cultivated in CCol-CI- and CsADM-CI-conditioned medium at different time durations; cell migration quantification of (d) HFCs and (e) HKCs. (scale bar represents 50  $\mu$ m, red represents nucleus staining DAPI and green depicts cytoskeleton expression). Y-error bars represent standard deviation, \*\* represent  $p < 0.01$ , and \*\*\* signifies  $p < 0.001$ .

130x161mm (300 x 300 DPI)

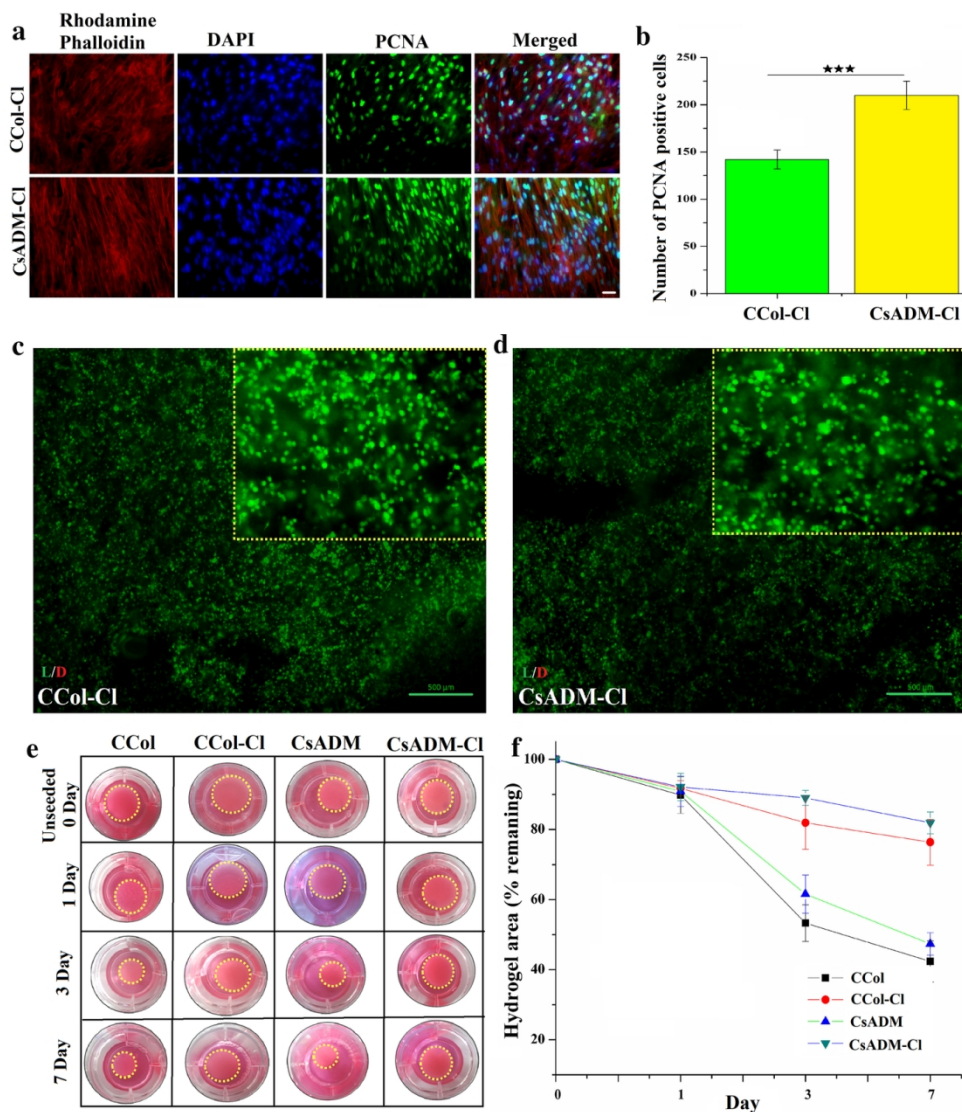


Fig. 5. Quantitative and qualitative cell infiltration and proliferation of HFC-encapsulated hybrid hydrogels. PCNA Staining images (a) and quantification of PCNA positive cells (b) of HFCs cultivated in C<sub>Col</sub>-Cl and C<sub>sADM</sub>-Cl. Live/Dead staining images of C<sub>Col</sub>-Cl (c) and C<sub>sADM</sub>-Cl (d) encapsulated with HFCs post 72 h of incubation; images of contraction of HFCs seeded hybrid hydrogels at different time period (e) and quantification of area remaining (f). Scale bar represents 50  $\mu$ m; Y-error bars represent standard deviation; \*\*\* signify  $p < 0.001$ .

127x143mm (300 x 300 DPI)

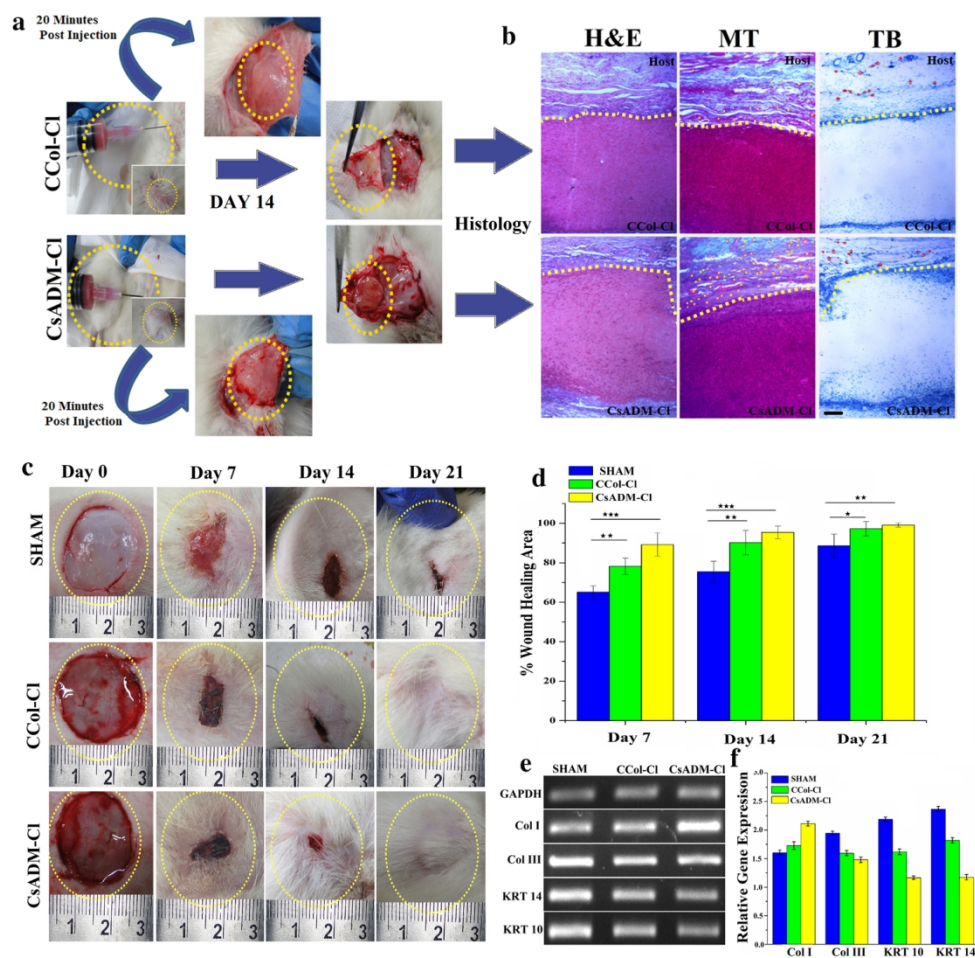


Fig. 6. Pre-clinical study in rat model. Biocompatibility of subcutaneously injected hybrid hydrogels (CCol-CI, and CsADM-CI) was evaluated in dorsal skin in rat model (a) and histological study post 10 days of injection (b). Healing progression of full-thickness cutaneous wounds treated with SHAM, CCol-CI, and CsADM-CI; optical images of wounds (c) and wound closure rate (d) on days 0, 7, 14, and 21; (e&f) RT-PCR analysis at 21-day post wounding. Yellow star represents blood vessel in MT staining (b), red star in TB staining represents TB positive stained cells (b), Yellow dotted line represent adjoining area between host and implant (b), Yellow circle area of interest (b), Scale bar represents 50  $\mu$ m; Y-error bars represent standard deviation, Yellow dotted circle represent wound area (c), \* signifies  $p < 0.05$ , \*\* signifies  $p < 0.01$ , and \*\*\* signifies  $p < 0.001$ .

132x130mm (300 x 300 DPI)



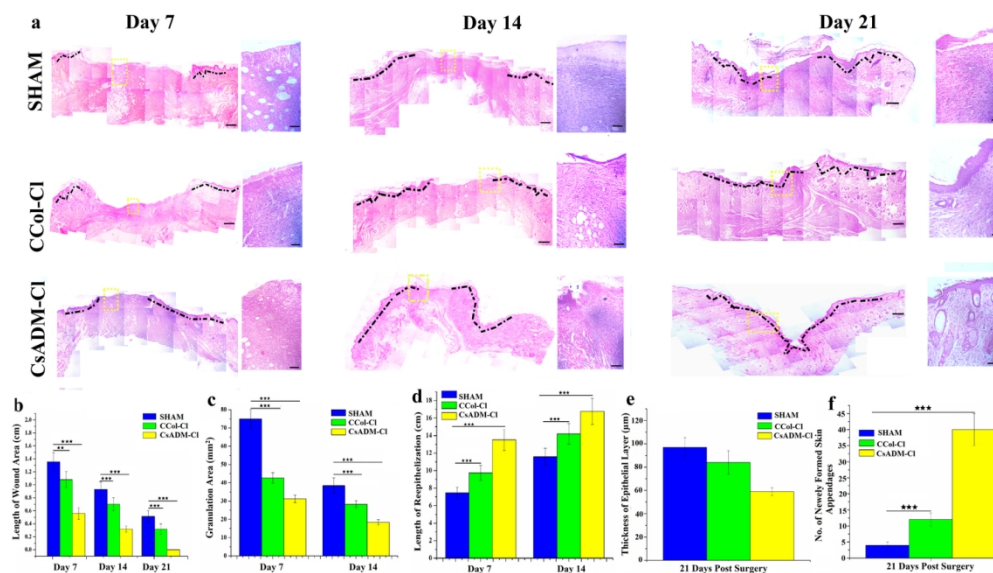


Fig. 7. Histomorphometric analysis provides quantitative wound healing efficacy of injectable hybrid hydrogels. Histological micrographs of wound sections implanted with CCol-CI and CsADM-CI at days 7, 14, and 21 after dermal excision by H & E staining (a), quantification of length of wound area (b), granulation area (c), length of reepithelization (d), thickness of epithelial layer (e), and no. of newly formed skin appendages at predetermined period (f). Scale bar represents 50  $\mu$ m; Black dotted line represent healed area; \*\* signifies  $p < 0.01$ , and \*\*\* signifies  $p < 0.001$ .

127x72mm (300 x 300 DPI)



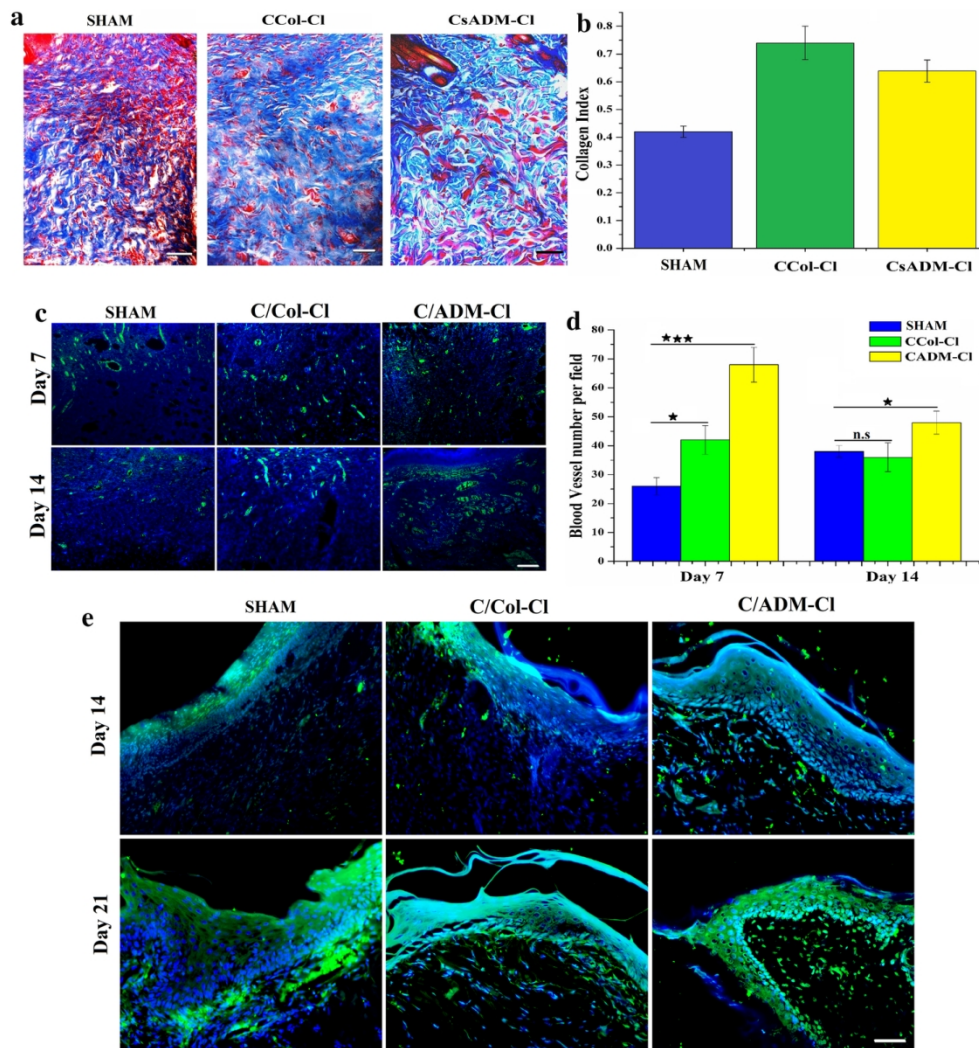


Fig. 8. Collagen staining and immunohistochemical analysis demonstrated the potential of the hybrid hydrogels to heal chronic wounds in rat model. MT staining (a) and quantification of collagen index (b) 21 days post treatment with CCol-CI and CsADM-CI. Representative immunohistochemistry images of anti CD-31 (c) and anti CK-10 (e) stained histological sections on determined periods. Quantification of blood vessels on day 7 and day 14 of wounds treated with SHAM, CCol-CI, and CsADM-CI (d). Scale bar represents 50  $\mu$ m; red represents nucleus staining DAPI, and green depicts antibody expression; Y error bar represent standard deviation; \*\* signifies  $p < 0.01$ , and \*\*\* signifies  $p < 0.001$ .

129x138mm (300 x 300 DPI)